

AD-A273 721



WL-TR-93-4054



**X-RAY COMPUTED TOMOGRAPHY
FOR EMERGING AEROSPACE MATERIALS
AND PROCESSES DEVELOPMENT**

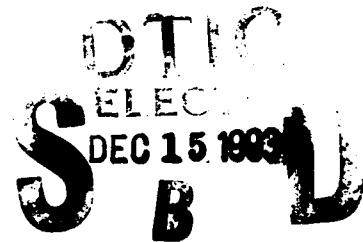
Richard H. Bossi
Gary E. Georgeson
Raymond D. Rempt

Boeing Defense & Space Group
P.O. Box 3999
Seattle, WA 98124-2499

May 1993

Interim Report for Period September 1991 to May 1993

Approved for public release; distribution is unlimited



6808

93-30318



MATERIALS DIRECTORATE
WRIGHT LABORATORY
AIR FORCE MATERIEL COMMAND
WRIGHT-PATTERSON AIR FORCE BASE, OHIO 45433-7817

93 12 14 046

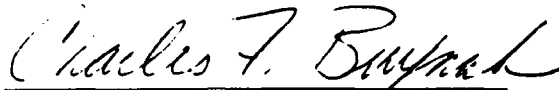
**Best
Available
Copy**

NOTICE

When Government drawings, specifications, or other data are used for any purpose other than in connection with a definitely Government-related procurement, the United States Government incurs no responsibility or any obligation whatsoever. The fact that the government may have formulated or in any way supplied the said drawings, specifications, or other data, is not to be regarded by implication, or otherwise in any manner construed, as licensing the holder, or any other person or corporation; or as conveying any rights or permission to manufacture, use, or sell any patented invention that may in any way be related thereto.

This report is releasable to the National Technical Information Service (NTIS). At NTIS, it will be available to the general public, including foreign nations.

This technical report has been reviewed and is approved for publication.


CHARLES F. BUYNAK
Nondestructive Evaluation Branch
Metals and Ceramics Division


TOBEY M. CORDELL, Chief
Nondestructive Evaluation Branch
Metals and Ceramics Division


for NORMAN M. TALLAN, Chief
Metals and Ceramics Division
Materials Directorate

If your address has changed, if you wish to be removed from our mailing list, or if the addressee is no longer employed by your organization please notify WL/MLLP, WPAFB, OH 45433-7817 to help us maintain a current mailing list.

Copies of this report should not be returned unless return is required by security considerations, contractual obligations, or notice on a specific document.

REPORT DOCUMENTATION PAGE			Form Approved OMB No. 0704-0188	
1. AGENCY USE ONLY (Leave Blank)	2. REPORT DATE May 1, 1993	3. REPORT TYPE AND DATES COVERED Interim September 1991- May 1993		
4. TITLE AND SUBTITLE X-Ray CT for Emerging Aerospace Materials and Processes Development			5. FUNDING NUMBERS F33615-88-C-5404 PE: 63112F PR: 3153 TA: 00 WU: 06	
6. AUTHOR(S) Raymond D. Rempt, Gary E. Georgeson, and Richard H. Bossi				
7. PERFORMING ORGANIZATION NAME(S) AND ADDRESS(ES) Boeing Defense & Space Group P.O. Box 3999 Seattle, WA 98124-2499			8. PERFORMING ORGANIZATION REPORT NUMBER	
9. SPONSORING/MONITORING AGENCY NAME(S) AND ADDRESS(ES) Charles Buynak (513) 255-9802 Materials Directorate (WL/MLLP) Wright Laboratory Wright-Patterson AFB, OH 45433-6533			10. SPONSORING/MONITORING AGENCY REPORT NUMBER WL-TR-93-4054	
16. SUPPLEMENTARY NOTES				
12a. DISTRIBUTION/AVAILABILITY STATEMENT Approved for public release; Distribution is unlimited			12b. DISTRIBUTION CODE	
13. ABSTRACT (Maximum 200 words) <p>The development and qualification of new materials and processes requires characterization of the product as a function of manufacturing and operational parameters. X-ray computed tomography (CT) provides quantitative measurements of material characteristics in terms of the dimensions, density and composition.</p> <p>The results of studies involving CT testing of various materials demonstrate the ability of CT to provide valuable information for material process understanding and characterization. The cost benefit of CT is found in the reduction of risk and schedule savings by reducing cycle time in process development steps. CT is a tool which increases new design options by allowing internal measurement and evaluation at previously inaccessible locations in complex structures. X-ray CT will be a critical tool for organizations competing in emerging materials and processes development.</p>				
14. SUBJECT TERMS Computed Tomography (CT), advanced materials, organic composites, honeycomb, ceramics, metal matrix composite (MMC), structural foam, bonds, process development, noninvasive micrography			15. NUMBER OF PAGES 68	
17. SECURITY CLASSIFICATION OF REPORT Unclassified			18. SECURITY CLASSIFICATION OF THIS PAGE Unclassified	19. SECURITY CLASSIFICATION OF ABSTRACT Unclassified
			20. LIMITATION OF ABSTRACT UL	

TABLE OF CONTENTS

Section		Page
1.0	INTRODUCTION	1
1.1	Computed Tomography	1
1.2	Scope and Objective	1
2.0	BENEFITS	3
2.1	Organic Composites and Advanced Materials	3
2.2	CT Benefits	3
2.3	Economic Factors	6
3.0	EXAMPLE STORIES	9
3.1	Adhesive Bonds	9
3.1.1	Multilayer Bond	9
3.1.2	Technique Development for Bonding Composite Substructure	13
3.1.3	Core to Internal Facesheet	18
3.2	Honeycomb Structure	20
3.2.1	Honeycomb Core Composites With Internal Septum	20
3.2.2	Water Presence in Honeycomb Panels	24
3.2.3	Honeycomb Panel with Internal Features	30
3.3	Difficult/Complex Structure	34
3.3.1	Graphite/BMI "V" Section	34
3.3.2	Sinewave Spar	37
3.4	Tows and Windings	40
3.4.1	Thick Composite Beam	40
3.4.2	Filament Wound Bottle with Foam Core	43
3.4.3	Wound Fiberglass Composite Ring	45
3.5	Material Density/Consolidation	47
3.5.1	Structural Foam for Spar Manufacture	47
3.5.2	Fibrous Ceramic Tile	50
3.5.3	High Temperature Coated Specimens	52
3.5.4	Aluminum MMC Rods	54
4.0	CONCLUSIONS	56
5.0	REFERENCES	58

DTIC QUALITY INSPECTED 1

Accession For	
NTIS GRA&I	<input checked="" type="checkbox"/>
DTIC TAB	<input type="checkbox"/>
Unannounced	<input type="checkbox"/>
Justification _____	
By _____	
Distribution/ _____	
Availability Codes	
Dist	Avail and/or Special
A-1	

LIST OF FIGURES

Figure		Page
2.3-1	Diagram showing how CT measurements can contribute to the activity of emerging material and process development.	8
3.1.1-1	CT image of bonds.	10
3.1.1-2	Enlarged area of interest from CT image of bonds.	10
3.1.1-3	Cylindrical coordinate presentation of the CT slice data.	11
3.1.1-4	Map of the disbond from a set of 22 contiguous CT slices.	12
3.1.2-1	Photograph of bonding jig.	13
3.1.2-2	Example CT image from trial 1 showing poor bonding.	14
3.1.2-3	Example CT image from trial 2 showing unbonds and ply disbonds.	15
3.1.2-4	Example CT image from trial 3 showing no unbonds.	15
3.1.2-5	Example CT image from trial 4 showing dry ply region but no unbonds.	16
3.1.2-6	UT Pulse echo C-scans of the bond area for trials 1 - 4	16
3.1.2-7	Average pull off strength versus trial number.	17
3.1.3-1	Photograph of a test section of a honeycomb composite enclosure.	18
3.1.3-2	CT slice taken below the edge in the foreground of the photograph.	19
3.1.3-3	CT slice taken perpendicular to the Figure 3.1.3-2 image.	19
3.2.1-1	Photograph of a section of a leading edge.	20
3.2.1-2	CT image showing septum.	21
3.2.1-3	CT image showing honeycomb.	21
3.2.1-4	Photograph of a honeycomb trailing edge.	22
3.2.1-5	CT image of honeycomb trailing edge.	23
3.2.1-6	Enlargement of Figure 3.2.1-5 showing bond line.	23
3.2.1-7	CT image showing variations along bond line.	24
3.2.2-1	Photograph of long honeycomb panel mounted on a CT system.	25
3.2.2-2	CT image showing water distribution in the honeycomb structure.	25
3.2.2-3	DR image showing water distribution in test panel prior to environmental cycling.	26
3.2.2-4	DR image showing water distribution in test panel midway through environmental cycling.	27
3.2.2-5	DR image showing water distribution in test panel after environmental cycling.	27
3.2.2-6	CT image of panel 2 showing water distribution in cells at 1.5 mm (0.06 inches) above the bottom preenvironmental cycling test.	28
3.2.2-7	CT image of panel 2 showing water distribution in cells at 2 mm (0.08 inches) above the bottom postenvironmental cycling test.	29
3.2.2-8	CT image across cells of panel 2 showing damaged cell.	29
3.2.3-1	Photograph of a composite test panel.	30
3.2.3-2	CT image of panel.	31
3.2.3-3	CT image parallel to Figure 3.2.3-2.	32
3.2.3-4	CT image of panel.	32
3.2.3-5	CT image across panel.	33
3.3.1-1	Photograph of "V" shaped composite test panel.	34

LIST OF FIGURES (Continued)

Figure		Page
3.3.1-2	CT image of "V" section showing artifacts.	35
3.3.1-3	CT image of "V" section using bolus to reduce artifacts for article 1.	35
3.3.1-4	CT image of "V" section for article 2.	36
3.3.1-5	Drawing showing region of interest and CT measurement results.	36
3.3.2-1	Photograph of a test section of a sinewave spar.	37
3.3.2-2	CT image of a sinewave spar.	38
3.3.2-3	CT image series of a sinewave spar showing flange cracks and delaminations. 39	
3.4.1-1	Photograph of a composite beam.	40
3.4.1-2	CT image of the composite beam.	41
3.4.1-3	MPR reconstructed CT image of the composite beam at 3.9 mm (0.15 inches) from surface.	41
3.4.1-4	MPR reconstructed CT image of the composite beam at 10.8 mm (0.43 inches) from surface.	42
3.4.1-5	MPR reconstructed CT image of the composite beam at 4.1 mm (0.16 inches) from surface.	42
3.4.1-6	MPR reconstructed CT image of the composite beam at 9.4 mm (0.37 inches) from surface.	43
3.4.2-1	Composite filament wound bottle with a foam core.	44
3.4.2-2	CT slice of the bottle.	45
3.4.2-3	CT slice of Figure 3.4.2-2 with contrast adjustment.	45
3.4.3-1	Photograph of fiberglass ring.	46
3.4.3-2	CT image of the ring showing voids in the windings.	46
3.5.1-1	Photograph of the five green specimens mounted for CT examination.	47
3.5.1-2	CT images of the "green" foam specimens.	48
3.5.1-3	CT image of the thermoformed foam specimens.	48
3.5.1-4	Density plots of "green" foam specimens.	49
3.5.1-5	Density plots for thermoformed foam specimens	49
3.5.2-1	Photograph of fibrous ceramic tile.	50
3.5.2-2	CT image in fibrous ceramic tile.	51
3.5.2-3	CT image in fibrous ceramic tile.	51
3.5.2-4	CT image in fibrous ceramic tile.	52
3.5.3-1	Photograph of two of the coated specimens.	52
3.5.3-2	CT image of specimens shown in Figure 3.5.3-1.	53
3.5.3-3	CT image taken perpendicular to Figure 3.5.3-2.	53
3.5.4-1	Photograph of Al MMC rods.	54
3.5.4-2	CT image of small aluminum MMC rod.	55
3.5.4-3	CT image of large aluminum MMC rod.	55
4.1-1	Emerging materials and processes conclusions.	56

LIST OF TABLES

Table		Page
2.2-1	CT Benefits for Organic Composites and Advanced Materials and Processes.	4
2.2-2	CT Limitations.	6
2.3-1	CT Economic Benefits.	7

ACKNOWLEDGEMENTS

The authors acknowledge the contribution of test materials and components provided by a variety of individuals from firms including General Dynamics, University of Alabama and Boeing Advanced Projects, Materials Technology, Manufacturing Research & Development, Military Airplane, B-2, and Helicopter Programs. Special thanks to Anna Baker, Bob Carlsen, John Dixon, Jim Eder, Dave Evans, Jennifer Holmquest, Larry Howard, Brad Kirkwood, Les Pence, Patrice Leptich, Jim Nelson and John Sullivan of Boeing. Scanning assistance from BIR is gratefully acknowledged.

DISCLAIMER

The information contained in this document is neither an endorsement nor criticism for any X-ray imaging instrumentation or equipment used in this study.

SUMMARY

Under final and demonstration task assignments of the Advanced Development of X-ray Computed Tomography Application program, computed tomography (CT) was evaluated for its benefits to companies involved in emerging materials and processing techniques.

The development and qualification of new materials and processes require characterization of the materials as a function of manufacturing and operational parameters. X-Ray computed tomography (CT) provides quantitative measurements of material characteristics in terms of the dimensions, density, and composition. The results of studies involving CT testing of various materials demonstrate the ability of CT to provide information needed in material process understanding. The cost benefit of using CT is in reduced risk and reduced cycle time for process development, resulting from easily interpreted nondestructive information on product condition being available at any or all intermediate stages in the process. By allowing internal evaluation for structures whose interiors are inaccessible by other nondestructive evaluation methods, CT increases design options and enables rapid evaluation of new design concepts. Organizations wishing to compete in advanced materials will find CT to be an essential tool.

CT system and operation costs are presently too high for routine examination of any but the most costly products. Rather, CT is an enabling technology for product development which will have inprocess quality control and/or very low cost final NDE. CT system costs will need to be reduced to the throughput costs of traditional NDI for CT to be implemented as an end item NDI tool. The geometry of many full scale aircraft composite and advanced material structures tends to be beyond the operational regimes of conventional (360°) access CT techniques due to the overall assembly size and aspect ratio. Because of this, CT primarily will apply to substructure, subsection testing, or small emerging material components.

1.0 INTRODUCTION

The goal of the Advanced Development of X-Ray Computed Tomography Applications demonstration (CTAD) program is to evaluate applications for which computed tomography (CT) can provide a cost-effective means of evaluating aircraft/aerospace components. The program is task assigned so that specific CT applications or application areas can be addressed in separate task assigned projects. This interim report is the result of task assignment studies. Under the program, candidate hardware is selected for testing that offers potential for return on investment for the nondestructive evaluation system and operation. Three categories of task assignment are employed in the program: 1) preliminary tests where a variety of parts and components in an application area are evaluated for their suitability to CT examinations for their inspection; 2) final tests where one or a few components are selected for detailed testing of CT capability; and 3) demonstrations where the viability of CT is evaluated and the results presented to government and industry. This interim report is the result of both a final and a demonstration task assignment study on the use of CT for emerging aerospace materials and processes. Additional task assignment reports that were issued by the CTAD program are listed in References 1 through 16.

1.1 Computed Tomography

X-ray computed tomography (CT) is a powerful nondestructive evaluation technique that was conceived in the early 1960's and has been developing rapidly ever since. CT uses penetrating radiation from many angles to reconstruct image cross sections of an object. The clear images of an interior plane of an object are achieved without the confusion of superposition of features often found with conventional film radiography. The CT images are maps of the relative linear X-ray attenuation coefficient of small volume elements in the object. The X-ray linear attenuation coefficient measurement is directly related to material density and is a function of the atomic number in the small volume elements. The volume elements are defined by the reconstruction matrix (in combination with the X-ray beam width) and by the effective CT slice height. The CT results can provide quantitative information about the density/constituents and dimensions of the features imaged.

Although CT has been predominantly applied to medical diagnosis, industrial applications have been growing over the past decade. Medical systems are designed for high throughput and low dosages specifically for humans and human sized objects. These systems can be applied to industrial objects that have low atomic number and are less than one-half meter in diameter. Industrial CT systems do not have dosage and size constraints. They are built in a wide range of sizes from the inspection of small jet engine turbine blades using midenergy (hundreds of keV) X-ray sources to the inspection of large ICBM missiles requiring high (MeV level) X-ray energies. Industrial CT systems generally have much less throughput than medical systems. The CTAD program uses a wide range of CT systems, both medical and industrial.

1.2 Scope and Objective

The task effort covered by this interim report involved the development and presentation of materials showing the useful application of CT to a variety of materials, processes, and their characterization. Organic composites and advanced materials, and their processes are the primary focus. A formal presentation of the CTAD program included this material at the Air Force Computed Tomography Applications Workshop held May 5-7, 1992 in Salt Lake City, Utah. In addition to the demonstration, educational materials on the application and benefits of CT were developed and included in the "Interactive Multimedia Presentation for Applied

Computed Tomography" (IMPACT) software that operates on Macintosh workstations. This package will be available from WL.

This task assignment also reports on additional example stories of CT benefits to materials characterization not reported in earlier task assignment reports. These examples include evaluation of bonded structures, large honeycomb structures with complex or difficult geometry, and material consolidation measurement.

2.0 BENEFITS

2.1 Organic Composites and Advanced Materials

Due to demanding requirements imposed on current and future high-performance aircraft structures, advanced materials and manufacturing processes are being developed for and used in a variety of applications to extend the range of performance available from traditional aerospace materials. Materials are often called "advanced" if they exhibit properties, such as high-temperature strength or high stiffness per unit weight, that are significantly better than those of more conventional structural materials, such as steel or aluminum. High strength-to-weight ratios and the ability to tailor the material to meet specific criteria (e.g., high stiffness in one direction) make organic composites highly attractive for these applications. In addition to organic composites, advanced materials include structural ceramics (also ceramic matrix composites (CMCs), polymer matrix composites (PMCs), metal matrix composites (MMCs), and new high-temperature/high-strength alloys. Processing techniques are also called advanced if they are new or innovative methods for basic material fabrication, joining, or assembly that create lower-cost and/or higher-performance products.

The key to advanced materials is that they are "tailored" to have the properties required for a given application. However, due to the nonhomogeneous nature of advanced materials (which are often a mixture of fibers or particulates and a matrix), problems arise in their manufacture and handling which result in defects unique to these materials, some of which can be hidden or uncharacterized. These defects include: delaminations, porosity, nonuniformities, fiber misalignment, improper layups or fiber volume fractions, honeycomb damage (in sandwich composites), facesheet/webbing disbonds, matrix cracks, and damage due to impact. In addition, many advanced material parts are complex, and, therefore, are difficult to inspect. Advanced structures may include channel shapes with tight radii, multilayered honeycomb structures, injection molded powder metal parts, and diffusion-bonded alloys.

Materials fabrication techniques are currently being developed and used which offer lower production costs than traditional methods. The materials are often made up of metals, alloys, or plastics. The parts manufactured by these methods can contain defects which are unique to the process and material. This development of emerging materials and processes is generating a need for improved quantitative nondestructive evaluation methods. Conventional qualitative methodologies (ultrasonics, radiography and visual) are proving inadequate to fully characterize and understand properties and defects of emerging materials and processes. Many advanced materials and manufacturing processes have experienced limitation in their quality evaluation because no adequate inspection method or acceptance criteria has been available.

2.2 CT Benefits

X-ray computed tomography provides cross-sectional images of test objects which are a map of the material X-ray linear attenuation coefficient of small volume elements defined by the image pixel size and CT slice thickness. These volumetric measurements are useful for feature detection, density measurement/constituent identification, and dimensional measurements. Table 2.2-1 lists some of the benefits of CT.

Table 2.2-1 CT Benefits for Organic Composites and Advanced Materials and Processes.

Problem	CT Benefit
Material Consolidation uniformity (mixture distribution) voiding porosity resin/fiber distribution dry ply flow characteristics	Quantitative measurement of density and variation over a 3D volume
Foreign Material	Detection, location, and quantification
Bonds (inaccessible to other NDE methods)	Location, extent, variations
Internal Structures/Reinforcements	Detection and measurement of placement, interface quality, shape, and condition
Damage & Testing (impacts, environment, loading, etc.)	Volumetric feature detection measurement
Coatings	Thickness, variation, interface quality
Anisotropic Fiber Structure	Fiber direction, tow alignment, wrinkles waviness
Dimensional Measurements	Noncontact, internal, external measurement
Repairs (honeycomb)	Adhesive location and amount

CT offers considerable potential to reveal three-dimensional quantitative information useful for design and manufacturing inspection and analysis. CT can precisely define the size and location of voids, inclusions, low density areas, and cracks within the inspected component. Depth information is useful in categorizing and evaluating defects. CT is sensitive to density variations, and can quantify gradient and material differences and can define the details of internal structure of complex configurations. Because complete spatial information on part configuration and defect location is available from CT, an engineering assessment of the as-built component is possible. Using CT data, engineers are able to obtain information that can be applied to problem solving in the development of new materials and processes.

Table 2.2-1 indicates that CT offers tremendous technical benefits to those involved in emerging materials and processes for evaluation of the condition of the product. However, there are limitations in the type of objects to which CT can be applied. Table 2.2-2 lists some of the technical limitations of CT. In general, CT is a volumetric measurement technique, so any feature to be detected must have adequate volume to be sensed. The CT system sensitivity to feature detail is a function of the design of the system. For systems designed to handle large parts (>250 mm (10 inches)), the inherent resolution is often in the range of 1 to 2 lp/mm (0.5 mm to 0.25 mm (0.02 to 0.01 inches)). The CT system will detect smaller features, such as narrow delaminations, provided there is sufficient material contrast, although the delaminations may not be resolved (i.e., separated from a close neighboring delamination). As the part to be inspected becomes smaller in size (< 250 mm (10 inches)), the CT system can be designed to provide greater resolution, typically in the range of 1/500 of the part size. Image artifacts can be a problem with product designs that have large aspect ratio (greater than 15:1). Because of this and the requirement that CT have access to 360° about a part, CT is not applicable to large, relatively flat, aircraft structures. Artifacts in some high-aspect ratio parts can be reduced with the use of a bolus material which fills in around the narrow section of a part to make the part appear as an object with more cross-sectional area than it actually has. CT does require adequate signal strength for the X-ray measurements, and this is affected by the X-ray energy/output, scan time and part material combination. For large objects, getting adequate signal requires expensive capital equipment.

Table 2.2-2 CT Limitations

CT Attribute	Technical Limitations
Volumetric Measurement	Disbond must have separation.
Detail Sensitivity Resolution	<p>Large structures: typically 0.5 mm (0.02 inches) features are resolved, smaller high contrast features can be detected.</p> <p>Small structures: (< 250 mm (10 inches)) typically resolves 1 to 2 parts in 500.</p>
Density Measurement	Multiple materials must differ in X-ray linear coefficients (density and atomic number) for detection (0.01% are typical for large, > 1mm, areas).
Artifacts	Large aspect ratios cause streak artifacts. (> 15:1 is difficult)
Part Handling Penetration	X-ray transmission limited by size, density, atomic number of part and the X-ray energy available.
Size/shape	Access to 360° around part is required.

2.3 Economic Factors

A primary goal of emerging aerospace materials and processes development is low-cost manufacture. This means that the quality inspection will be built into the process or the process will use a high-speed, low-cost NDE method. Present CT technology is too costly for routine end-item inspection (except for very high value parts, such as rocket motors and nozzles). Therefore, CT is primarily applied as an enabling tool for the development of the new materials and processes. The education of engineers to the technical benefits of CT will lead to the effective utilization of CT measurements, with real economic benefits to the overall product. The application of CT is driven by unknowns in the new material and processes activities which only CT measurements can adequately provide.

Table 2.3-1 summarizes the economic benefits of CT, which are reduction of cycle time, reduction of risk, and increased design options. The example stories of using CT on product development activities in the CTAD program have identified significant benefits in a number of cases. Estimates of direct cost saving for emerging material and process activities, however, are unreliable because the economic factors are extremely difficult to quantify for new product developments. Because the Table 2.3-1 benefits are very difficult to quantify, the use of example stories is the method selected to provide engineers with a means to gauge the potential economic value of CT measurements to their programs.

Table 2.3-1 CT Economic Benefits

Global Contribution of CT	Economic Value
Improves information on part quality and process effects	Reduces Development Time Reduces Risk
Allows measurements in complex structures	Increases Design Options

Based on the experience of the CTAD stories, it is possible to construct a general comparison of CT as an enabler of product development versus approaches that use traditional measurement techniques. Figure 2.3-1 shows graphically how CT can contribute to the activity of emerging material and process development. In this figure, the traditional approach requires a number iterations (design, prototyping, evaluation, testing, redesign, etc.) for the development team to arrive at sufficient information to establish the final product configuration (i.e. materials and processes) that provides the desired result. With CT, quantitative measures obtained nondestructively for features, consolidation, and dimensions within the product are available. This easily interpreted information allows informed decisions for product/process changes to rapidly define and achieve the desired final configuration and quality. The number of iterations to reach the necessary information level required for final product definition will be reduced. The graph of Figure 2.3-1 shows generalized curves for the relative effects of using CT versus the traditional (lack of quantitative nondestructive data) approach. By employing quantitative measurements, the overall product development schedule will be improved. The amount of improvement to the overall process, through the application of CT, will depend on the specific product.

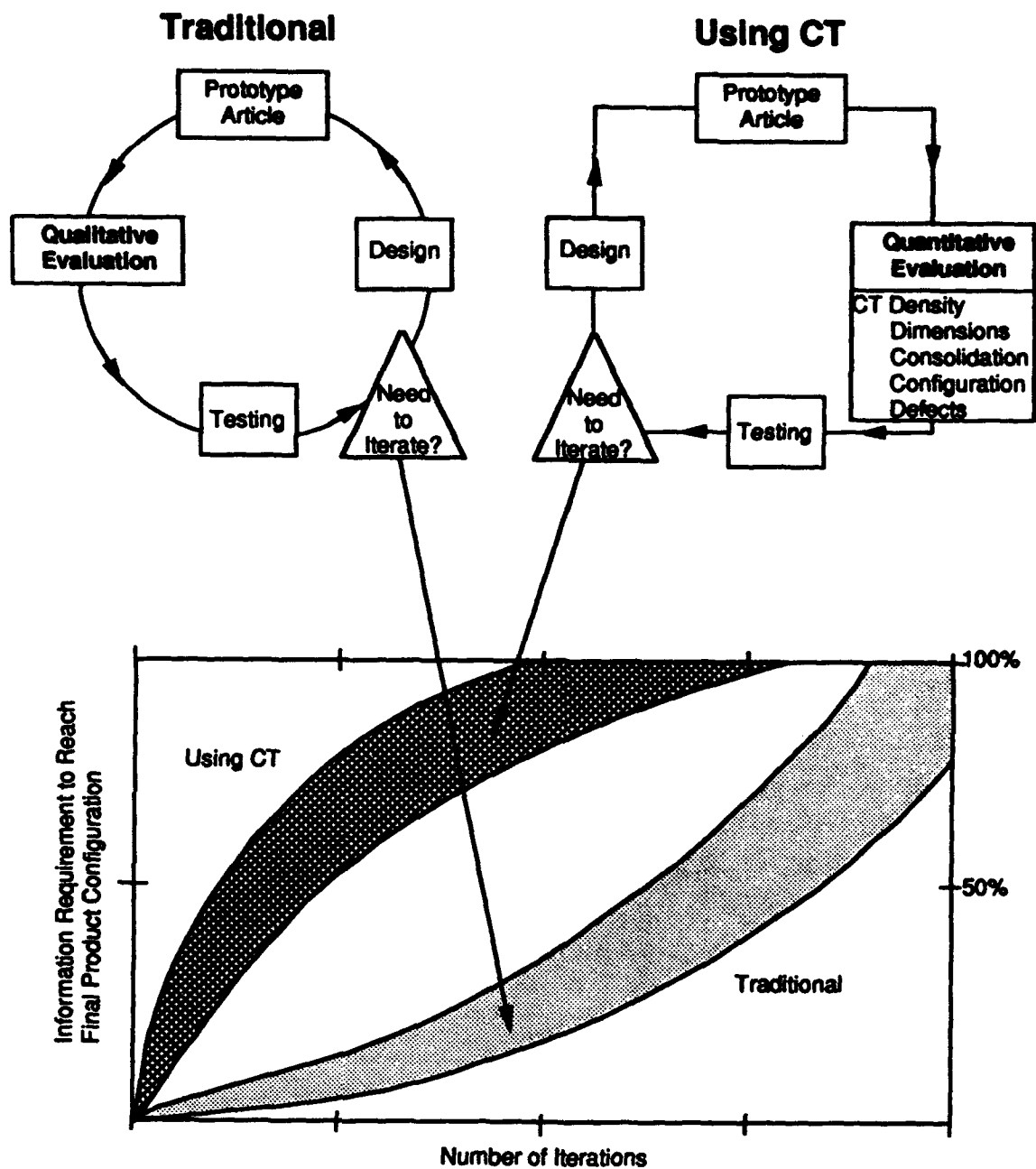


Figure 2.3-1 Diagram showing how CT measurements can contribute to the activity of emerging material and process development.

3.0 EXAMPLE STORIES

The CTAD program showed that CT can be cost effectively applied to product and process development for organic composites and advanced materials. The mechanism for introducing individuals, involved in these emerging materials and processes development activities, to the benefits of CT, was through example stories. This section includes example stories on adhesive bonds, honeycomb structure, difficult/complex structures, fiber tows and windings, and material density/consolidation measurements not previously reported in earlier interim reports.

3.1 Adhesive Bonds

Adhesive bonding offers many benefits for reducing assembly costs and improving structure designs. Unfortunately, no suitable NDE technique, including CT, exists for measuring the final bond strength. However, CT offers measurements of physical contact, bondline thickness, shape, and voiding that are valuable for process control and property prediction.

3.1.1 Multilayer Bond

A particular problem in bonded structures is when bonds lie on multiple layers or behind shapes that make ultrasonic testing (UT) access and interpretation difficult. An example is a bond on a conically shaped composite part, selected from an existing Boeing development program. The structure has two adhesive bonds, one between the conical structure and a spacer block, and a second between the space block and the attachment block. Ultrasonic examination is very difficult because of the unusual shape of the spacer; and, although access is possible for some regions of the bonds through the attachment block, the bond for the cone bond to spacer block is inhibited by the presence of the spacer to attachment block bond. CT scans were made across the circular cross section of the structure (the cone inner diameter is approximately 180 mm (7 inches)), revealing the bond assembly and presence of disbonds. A typical slice is shown in Figure 3.1.1-1. The disbonds are evident between the cone and the space block on the right, and also between the spacer and attachment block. Figure 3.1.1-2 shows an enlargement of one side of the structure where disbonds are present. In this figure, a system of coordinates on the part was defined in order to prevent the ambiguity often presented by non-part-specific coordinates. The dark dots at several locations in the bonds in Figure 3.1.1-2 are spacer wires. Because of the two disbonds, it is not possible to successfully evaluate the cone-to-spacer-block bond extent with normal UT methods when the only access is at the attachment block. CT also allows each bond to be evaluated individually over the length of the bond by taking successive CT slices and reconstructing the data in a plane perpendicular to the original CT slice plane. The larger of the disbonds was studied in detail in this manner.

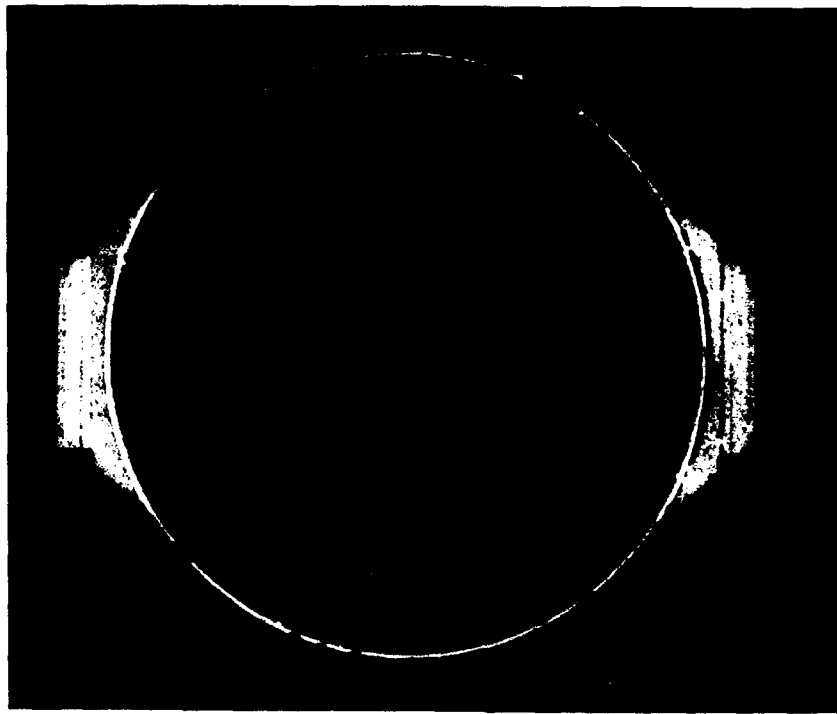


Figure 3.1.1-1 CT image of bonds.

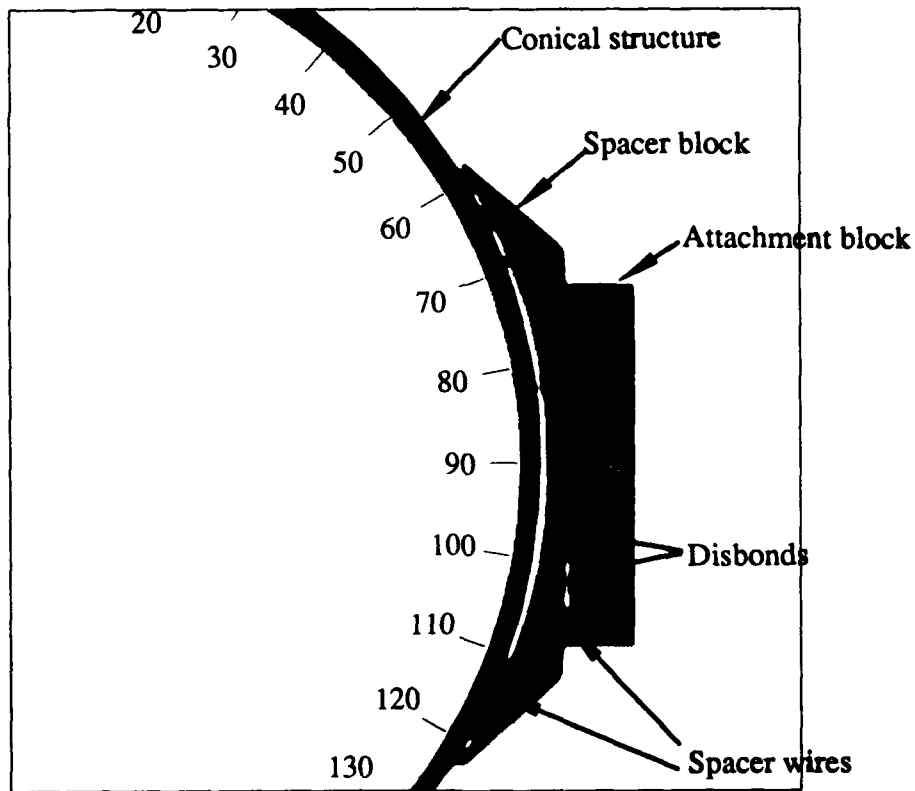


Figure 3.1.1-2 Enlarged area of interest from CT image of bonds.

The data from this CT slice can be presented in a cylindrical (radius and theta) coordinate system mapped onto rectangular axes, as shown in Figure 3.1.1-3. The data is distorted in the r (radius) direction due to the magnification in that direction and "warping" of the inside wall of the cone when mapped onto the rectangular axis. The grayscale thresholds were set to make densities less than that of the composite material (e.g., air) appear white and those greater to appear black. The disbond is seen as the white area on the left hand portion of the figure, in the attachment region. The dark vertical lines in the gray area of the figure are the wires whose cross-sections have been "warped" into lines. Figures 3.1.1-2 and 3.1.1-3 indicate that the width of the disbond in the radial direction is roughly equal to the diameter of the inserted wires.

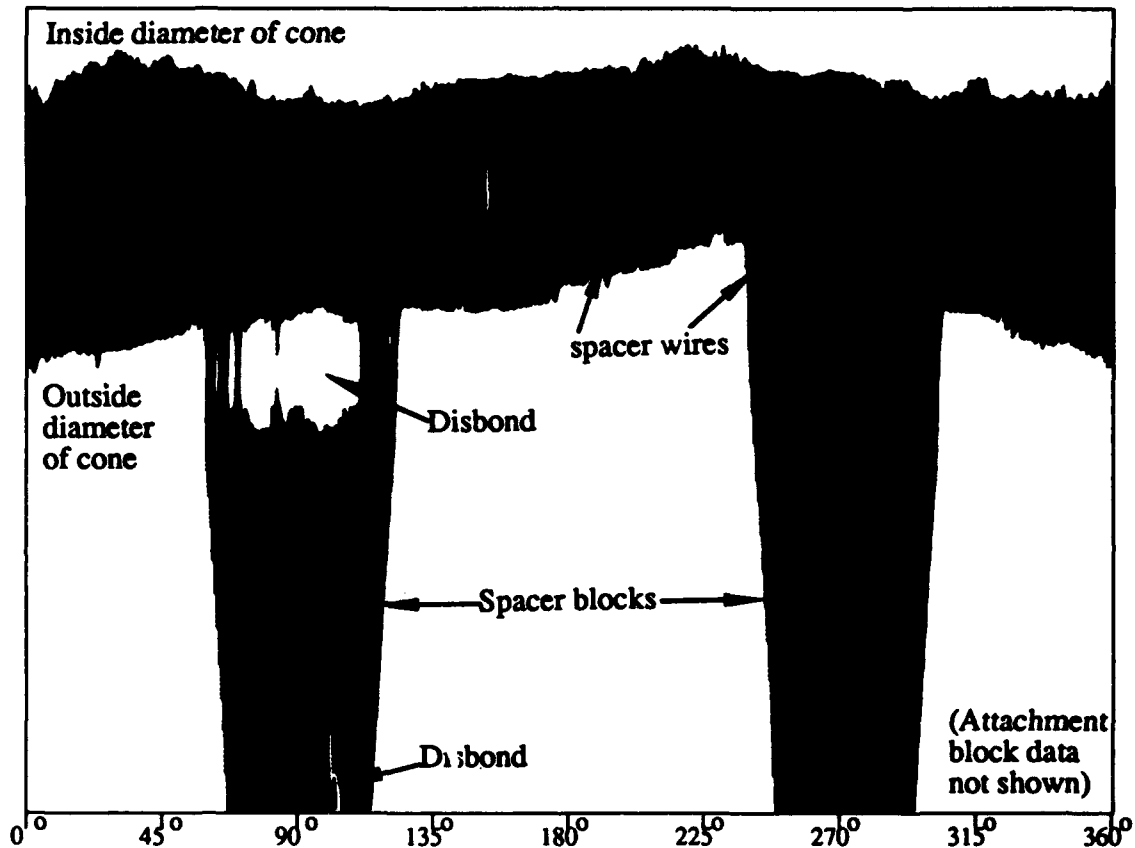


Figure 3.1.1-3 Cylindrical coordinate presentation of the CT slice data.

A series of 22 slices was taken at 2-mm intervals along the axis of the conical structure to create a volume data set. The data from these contiguous slices were processed to produce a "map" of the disbond in the vertical (z) and angular (theta) plane. By plotting the minimum through-thickness density for this plane from the volume CT data set, the disbond area will appear in the image as a function of angle and vertical height. The minimum CT density in the radial direction over the region of the bond is the disbond, i.e., the air in the disbond is seen as low density with CT. The plot is shown in Figure 3.1.1-4. This presentation of the composite data from all of the slices is essentially a map of the disbond and can be used to directly determine its area.

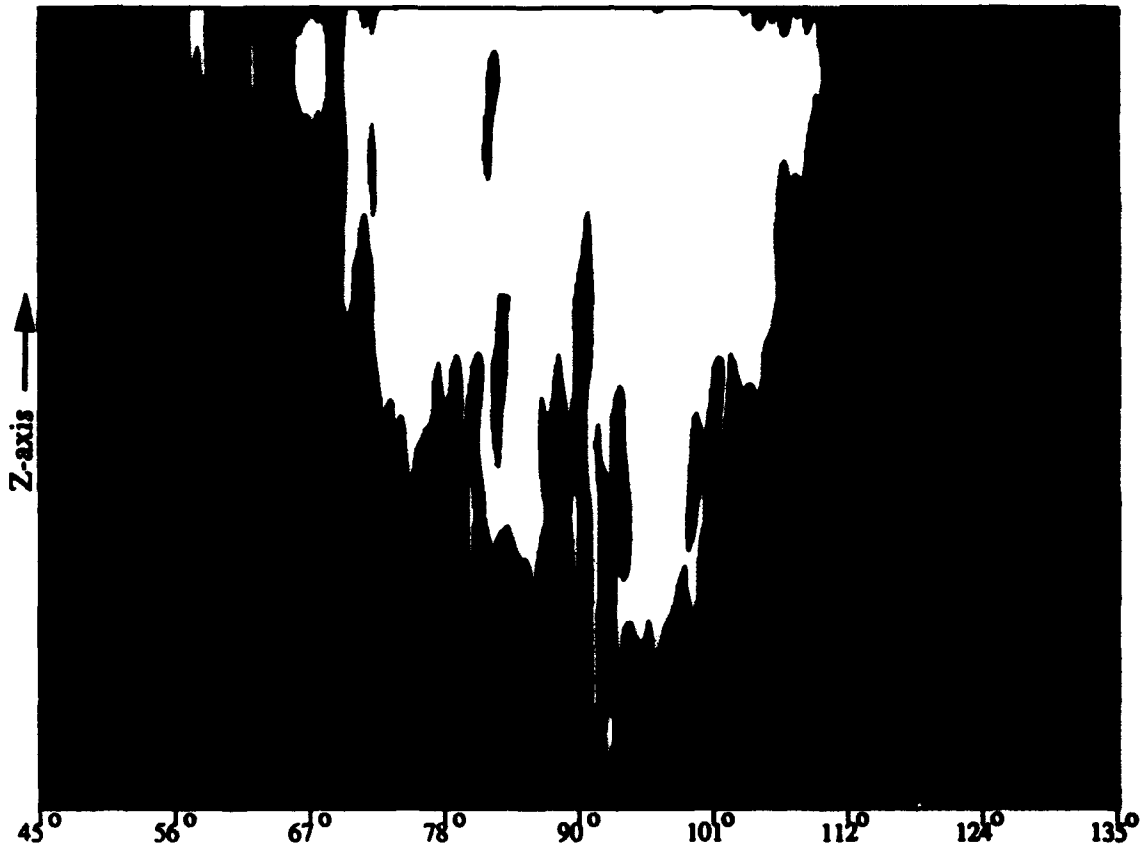


Figure 3.1.1-4 Map of the disbond from a set of 22 contiguous CT slices.

This is a good example of how CT removes ambiguity from an otherwise confusing situation. In addition to positively distinguishing between flaws, detailed evaluation of selected flaws is still routinely achievable. In addition, data reduction processes such as this are easily automated enabling routine evaluation without significant added labor costs.

3.1.2 Technique Development for Bonding Composite Substructure

Adhesive bonding of substructure to skins in aircraft/aerospace applications generally requires an autoclave in order to provide the temperature and pressure necessary for the curing of the high-strength adhesive. This requirement places access constraints on the program manufacturing the structure, and size and configuration limitations on concepts utilized in the design. Autoclave usage is also costly, and multiple cycles are often required to build up all but the simplest of structures. Vacuum bagging of composite structures to allow for ply compaction or bondline pressure can also limit the design and be very time consuming. Adhesive bonding methods which eliminate the need for bagging and the autoclave will allow a great deal more design and manufacturing freedom than is currently available. A technique for adhesively bonding previously cured spars and skins without the use of vacuum bagging or the autoclave employed CT to assist in the testing and analysis of bonding "T" spars to panel sections using a specially designed jig. CT enabled progressive improvement in the bonding method for each successive bond trial by providing key information about the bonds, such as bondline width, contact, and porosity. Tensile pull-off tests were performed on sections cut from the spar/skin combinations at CT slice locations. The results showed that a consistent, uniform bond could be made with this method.

Figure 3.1.2-1 is a photograph of a bonded T-spar-to-skin section. The jig, constructed for demonstrating out-of-autoclave bonding is designed to allow adhesive bonding of 65-mm-wide composite "T" spars to 250-mm-wide skin sections.

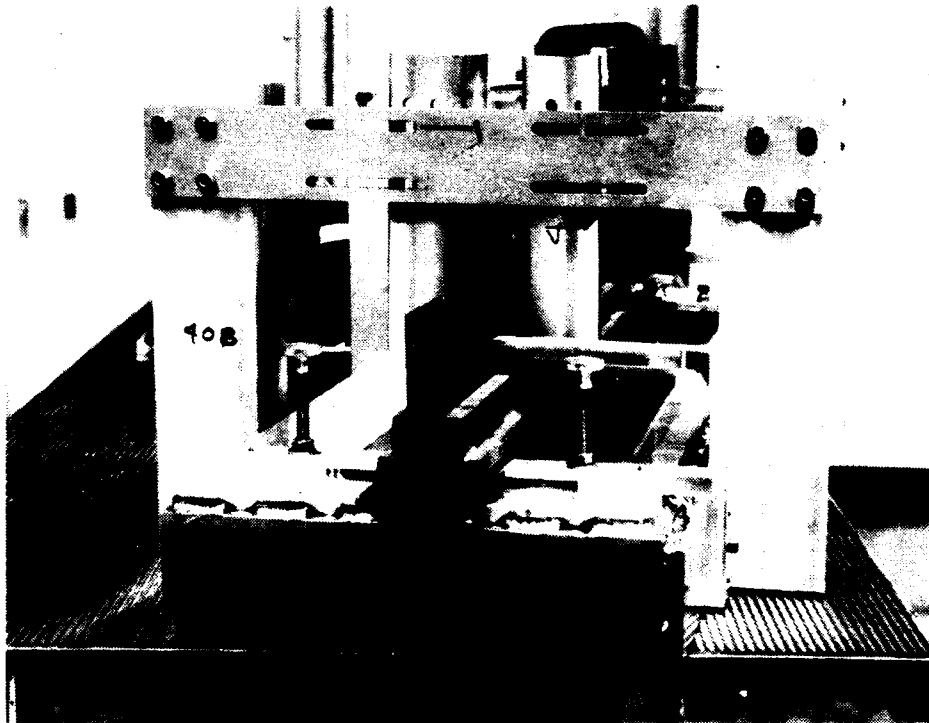


Figure 3.1.2-1 Photograph of bonding jig.

Four bond trials were planned and run as part of a test program. Each test was evaluated for technique and the bond quality produced, as measured by nondestructive and destructive testing. Ultrasonic testing, destructive sectioning, and tensile pull tests were done after all the spar/skins were bonded, but the X-ray CT evaluation was performed after each bond test so that changes in the technique could be made for the subsequent test. CT "slices" were taken every 75 mm (3 inches) along the spars. Tensile specimens, 150 mm (6 inches) long, were cut at every other CT slice location, providing a correlation of CT measurement (at each edge and in the middle) with tensile strength once the specimens were pulled. The four bond trials represent a history of evaluation and analysis which demonstrated progressive improvement from the first set to the last.

The first bond trial used 50-psi pressure and a single sheet of adhesive, nominally 0.2 mm (0.008 inches) thick. The spar/skin configuration was examined carefully. CT evaluation clearly showed there were large unbond areas corresponding primarily to the locations of the thermocouple wires. Figure 3.1.2-2 is a CT slice taken parallel to a thermocouple wire, showing the unbond where the thermocouple did not allow the spar to lay completely flat (the thermocouple is not visible in the CT image). The white dots in the CT image are cross sections of the barium doped tows in the composite fabrication, used for verification of tow alignment with radiography.

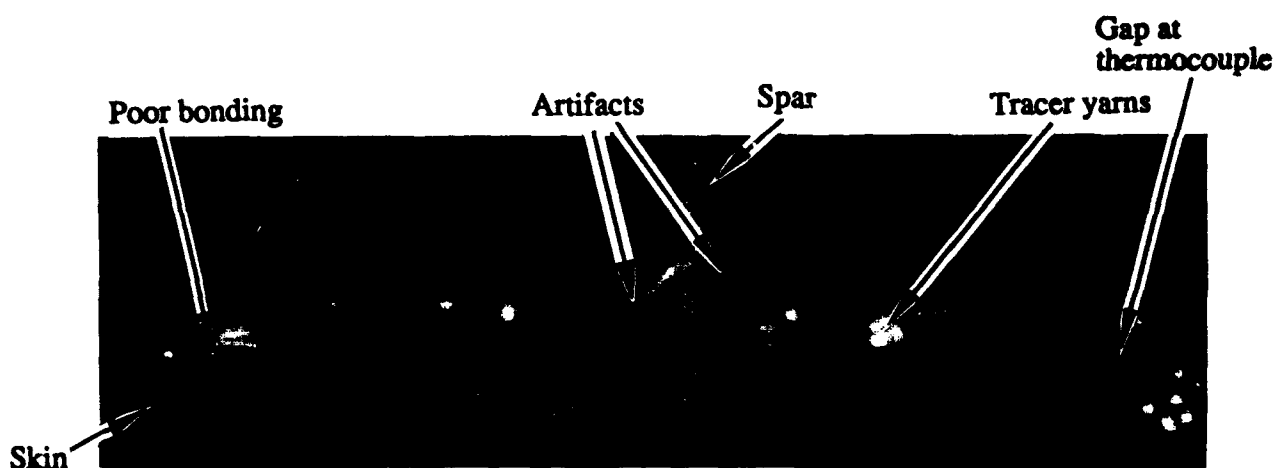


Figure 3.1.2-2 Example CT image from trial 1 showing poor bonding.

For the second trial the adhesive layer was doubled. Small grooves were cut into the second spar at the adhesive interface which decreased, but did not eliminate the bridging of the spar over the thermocouple wire. The bridging and lack of bonding were more isolated. A "glitch" in the temperature controller caused overheating of the bondline. An obvious "browning" of the adhesive was observed by visual inspection of the edge of the bond. CT analysis of this second spar/skin configuration revealed disbonding of the skin at various plies due to thermal breakdown of the composite. It also showed various areas where good bonding was not achieved. Figure 3.1.2-3 is an example of a CT image which indicated these features.

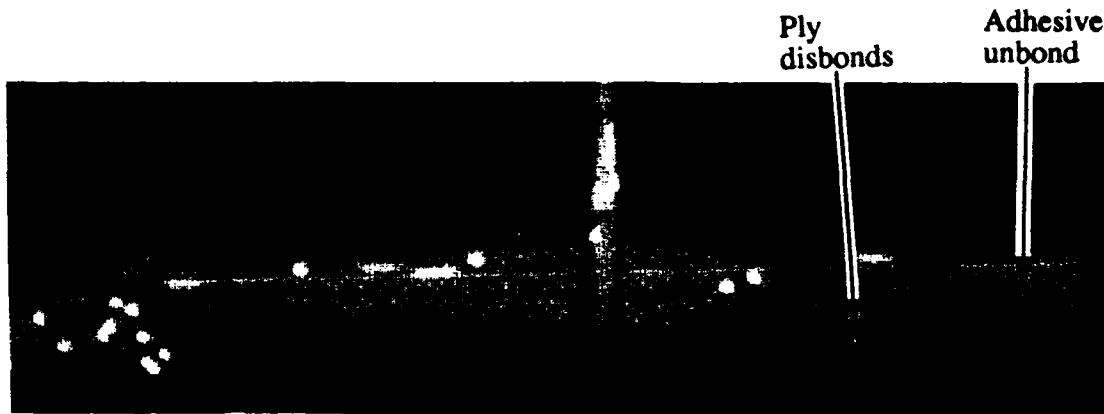


Figure 3.1.2-3 Example CT image from trial 2 showing unbonds and ply disbonds.

For the third bond trial, the controlling thermocouple was embedded in the bondline at the extreme end of the spar, and the thermocouple in the center of the spar was placed on top of the flange rather than in the bondline. This eliminated any potential bridging of the spar due to thermocouple wires in the central section of the spar. The CT results indicated a good contact along the bondline. An example is Figure 3.1.2-4.

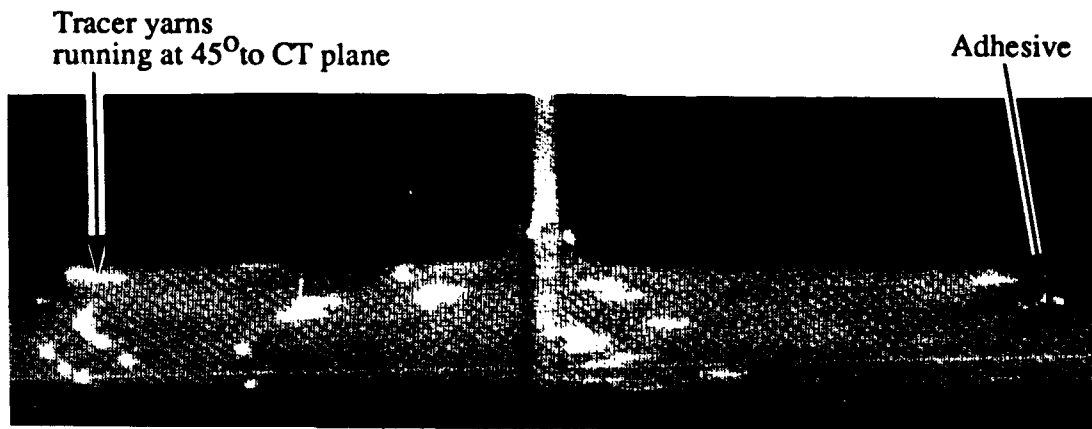


Figure 3.1.2-4 Example CT image from trial 3 showing no unbonds.

The fourth bond trial was run with a single adhesive film, nominally 0.2 mm (0.008 inches) thick, and an increase in air pressure in the elastomeric (65 psi). The purpose of these changes was to determine if a good bond could be made with less adhesive but more pressure. The CT results indicated a good contact all along the entire length of the bondline. However, a dry ply indication was identified along most of the length of the spar on one side of the flange which can be seen in the CT image of Figure 3.1.2-5.

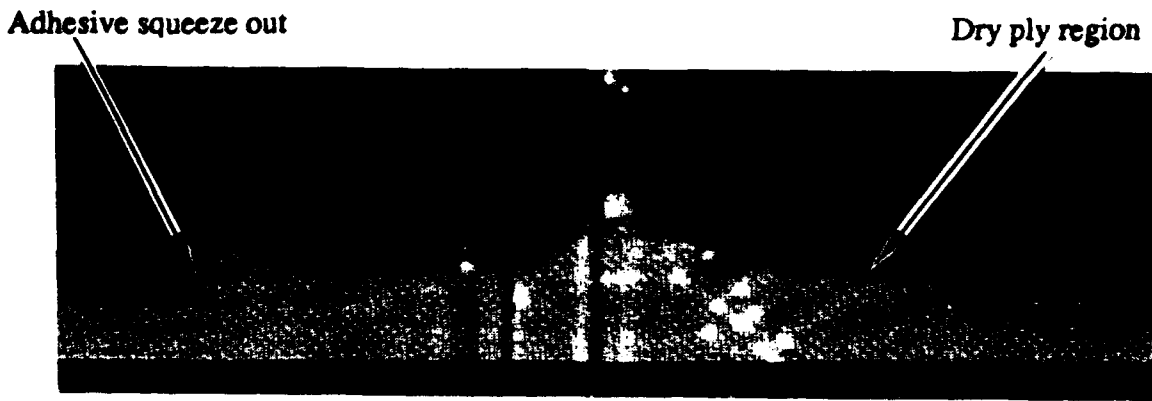


Figure 3.1.2-5 Example CT image from trial 4 showing dry ply region but no unbonds.

Once the bond trials were completed, ultrasonic inspection of the bondlines was conducted for the four spar/skin elements. Like the CT results, the UT data indicated a progressive improvement in the bond quality of the samples from 1 to 4. Unlike CT, however, the UT data did not provide any clear information as to why the differences occurred. The pulse echo ultrasonic C-scan images of the four elements are shown in Figure 3.1.2-6. The dark areas represent ultrasonic signal reflected from the bondline and indicate a good bond. Sample 1 has a random pattern of disbonds and exhibits the least consistent bondline of the four. Sample 2 has indications of bondline voids and unbonds, especially on the side with the thermocouple wires. Samples 3 and 4 show a dramatic increase in the good bondline area.



Figure 3.1.2-6 UT Pulse echo C-scans of the bond area for trials 1 - 4, taken at 2.25 MHz from the flange side of the bond. Dark areas represent regions where the ultrasonic path is maintained across the bond.

The UT results pointed to the same general conclusions about the bond quality of each sample. UT was helpful in providing information within the bond plane (percent good bond). However, unlike CT, UT could not provide the cross-sectional information on the bondline which showed why a bond was poor (lack of spar/skin contact, spar warpage, separation due to thermocouple placement, too little adhesive, etc.). CT provided the type of information that could drive the decision making process. After examining the CT data on one of the bond test elements, an engineer on the program commented that UT was not really necessary [during technique development] because CT could tell him what he needed to know for process decisions. UT was then used as a supplement after the bonding tests were completed.

All four spar/skin were cut into 6-inch sections for the purpose of tensile pull-off tests. The sectioning was done with a diamond grit-coated band saw at locations where the CT slices had been taken. Visual inspection of the edges of the individual sections verified the CT results and interpretation for each spar. Pull-off tests were conducted using an MTS 850 material testing system. The primary goal of these tests was to establish that a consistent bond along the length of the spar could be made with the bond jig. Also, the testing was to provide some correlation of bond strength to the bonding parameters chosen during each test.

The pull-off results reflected the progressive improvement of the bonding technique from trial 1 to trial 3 that was indicated by the CT analysis. Trial 4 contained dry plies which caused the part to fail before the bondline failed. Figure 3.1.2-7 is a graph of the average pull-off strength versus test number for three of the four spar/skin tests. This graph illustrates that the out-of-autoclave bonding process can be controlled and improved. This result was predicted based upon the CT data.

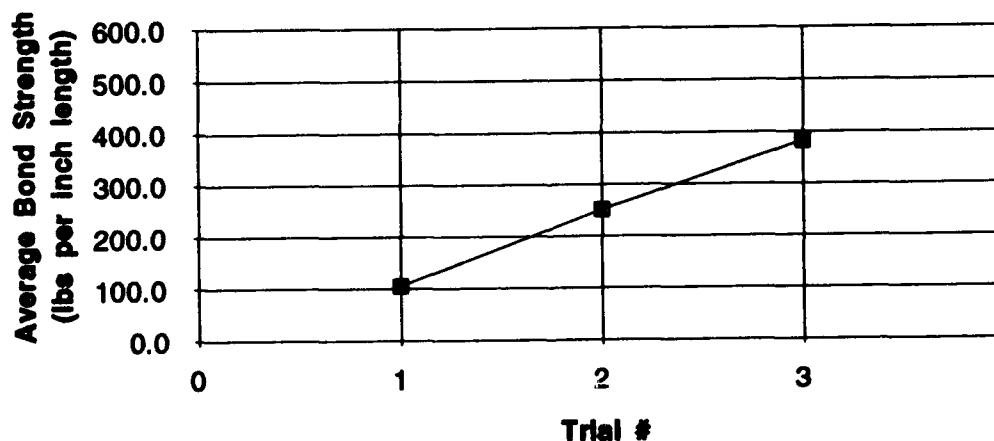


Figure 3.1.2-7 Average pull off strength versus trial number.

The results of this effort indicated that an out-of-autoclave bonding scheme for bonding composite aircraft structure is feasible. CT demonstrated its usefulness in both systematically establishing and evaluating the bonding process. With CT, a good bonding practice could be developed and the bond itself could be evaluated accurately and quantitatively. CT saved both time and money, though the nature of the savings makes it difficult to quantify.

3.1.3 Core to Internal Facesheet

It is often quite difficult to successfully detect defects on the interior wall of thick-walled honeycomb structures using normal NDE methods because the interior wall is inaccessible or the honeycomb is too dispersive for modalities such as ultrasonics. If the structure is of a suitable size for mounting on a CT system, it is possible to use CT to evaluate features of the internal bond surface. Figure 3.1.3-1 shows a photograph of a section of a honeycomb composite enclosure. The enclosure itself is curved, as is shown in the figure, and is slightly more than 50 mm (2 inches) thick. On the photograph a disbond is indicated whose extent has been mapped thermographically.

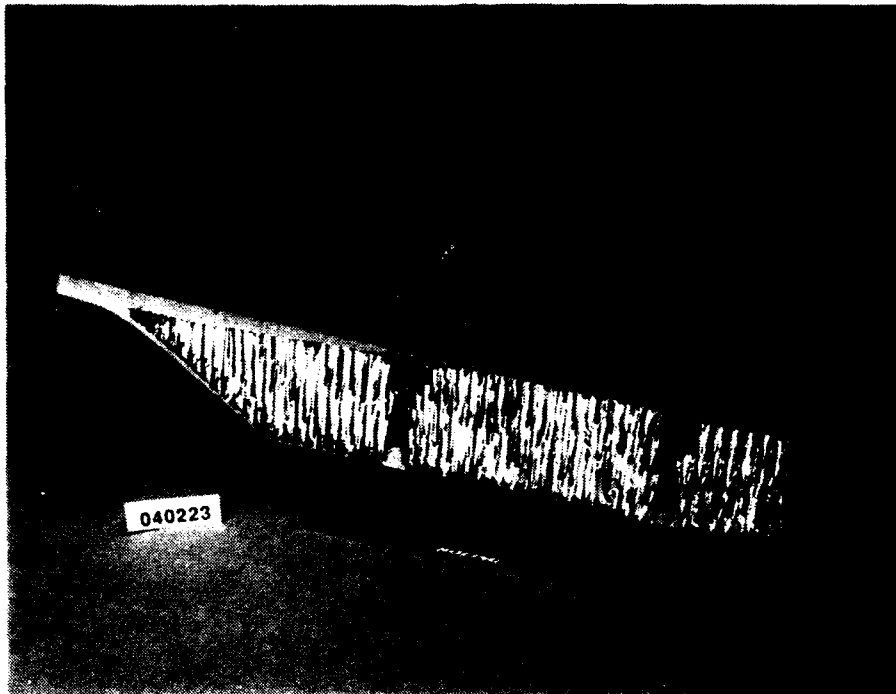


Figure 3.1.3-1 Photograph of a test section of a honeycomb composite enclosure.

CT scans of the defect were taken in two mutually perpendicular planes, each normal to the surface underwhich the disbond exists. If the entire enclosure were present, rather than just a section, the CT slices could have been made in precisely the same way, provided the scanner and part size were matched. Figure 3.1.3-2 is a CT slice taken below the edge in the foreground of the photograph. The slice indicates the disbond, as well as foaming adhesive in the top of the vertical void and some filler material in the bottom of the void.

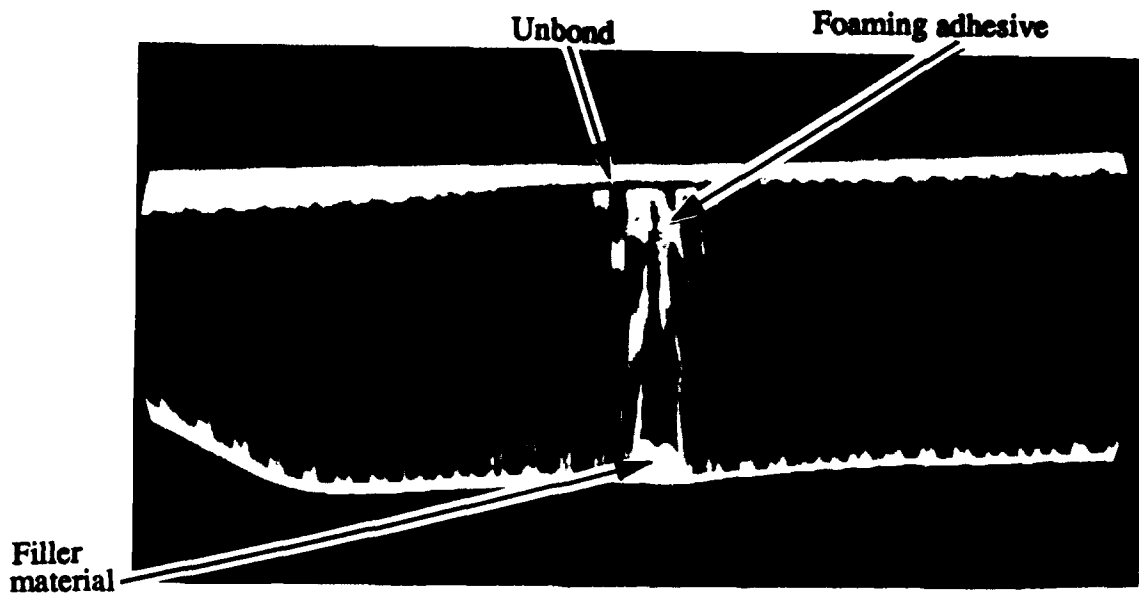


Figure 3.1.3-2 CT slice taken below the edge in the foreground of the photograph.

Figure 3.1.3-3 is a CT slice taken through the curved section perpendicular to the CT slice in Figure 3.1.3-2. From this slice it is easy to see that the disbond extends more than halfway across the section; whereas, thermographic mapping indicated an extent of less than one quarter of the way across. This information can be critically important to the successful development of processing techniques and monitoring measurement results from alternative methods.

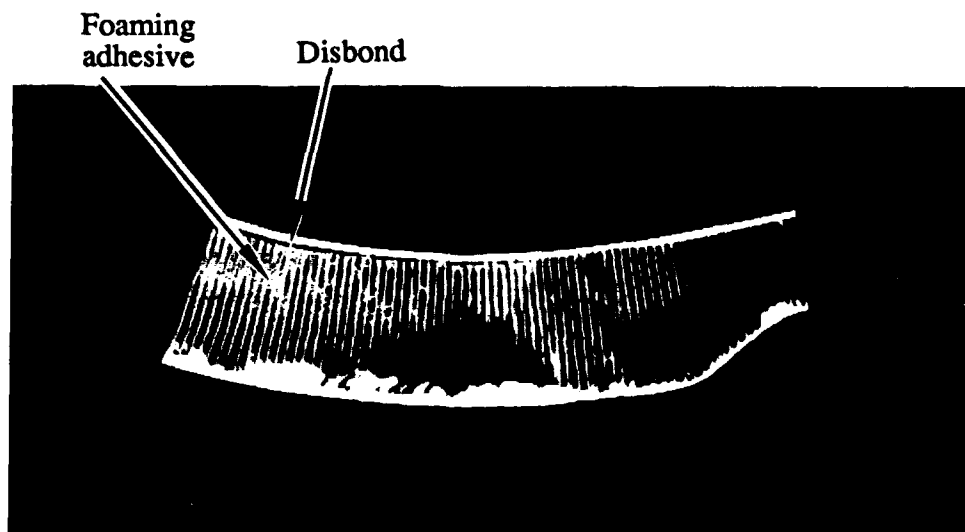


Figure 3.1.3-3 CT slice taken perpendicular to the Figure 3.1.3-2 image.

3.2 Honeycomb Structure

Honeycomb offers advantages in the manufacture of lightweight, high-strength structures. The development of large honeycomb structures requires the definition and control of the manufacturing assembly and bonding variations that can occur.

3.2.1 Honeycomb Core Composites With Internal Septum

Because of their high strength-to-weight ratio, honeycomb structures have advantages for performance over traditional structures. But, they can be difficult to inspect for internal bond conditions, particularly at internal septa. Several such composites were examined with CT under the CTAD task assignments.

One example is a leading edge made from a nomex honeycomb core bonded to a fiberglass skin. The core contains several internal septa, including one with a copper layer, to which the honeycomb material is bonded. A section of this leading edge is shown in Figure 3.2.1-1, illustrating the composite skin, honeycomb core and the various septa. The section includes a hole normal to its axis. The complexity of the geometries, as well as the number of different materials, limits the applicability of traditional NDI methods such as UT or ET.

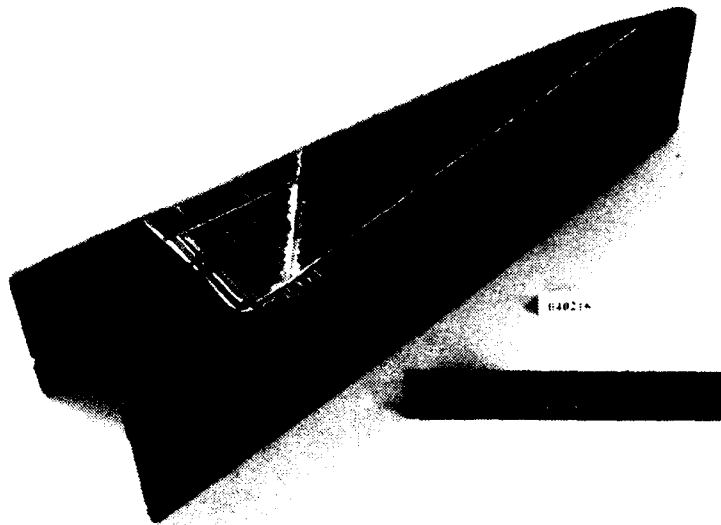


Figure 3.2.1-1 Photograph of a section of a leading edge.

Several CT slices of the section were taken to evaluate the quality of the adhesive bond between the septa and the honeycomb material, and to check for internal damage to the honeycomb material itself. One slice, whose image was displayed for two different values of density window width and density window level, revealed useful information regarding both the adhesive bond and the honeycomb condition. As shown in Figure 3.2.1-2, the bonding is uniform on the interface between the septa and the honeycomb material. Decreasing the density-window width and level revealed core damage to the interior of the honeycomb, in the triangular region bounded by the septa and the composite stiffener. This is shown in Figure 3.2.1-3. The black horizontal streak running near the upper surface is an image artifact, and not indicative of any condition of the material.

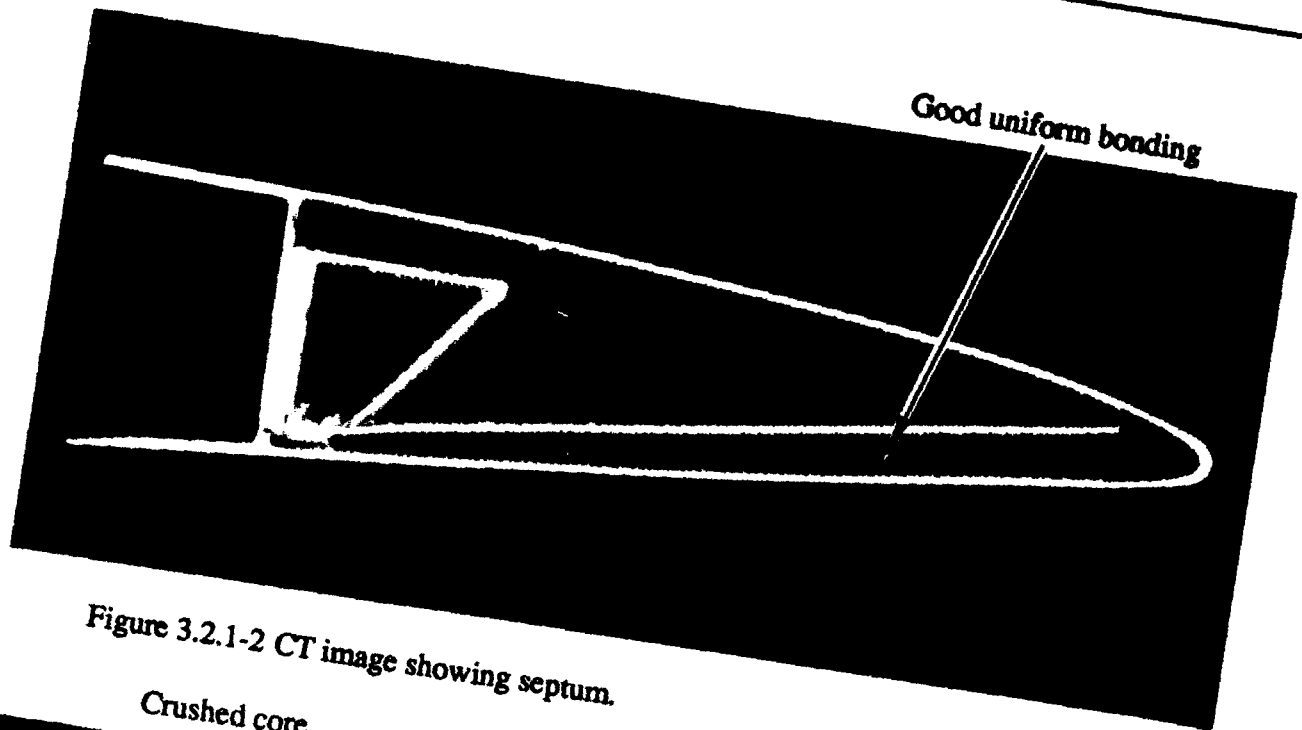


Figure 3.2.1-2 CT image showing septum.

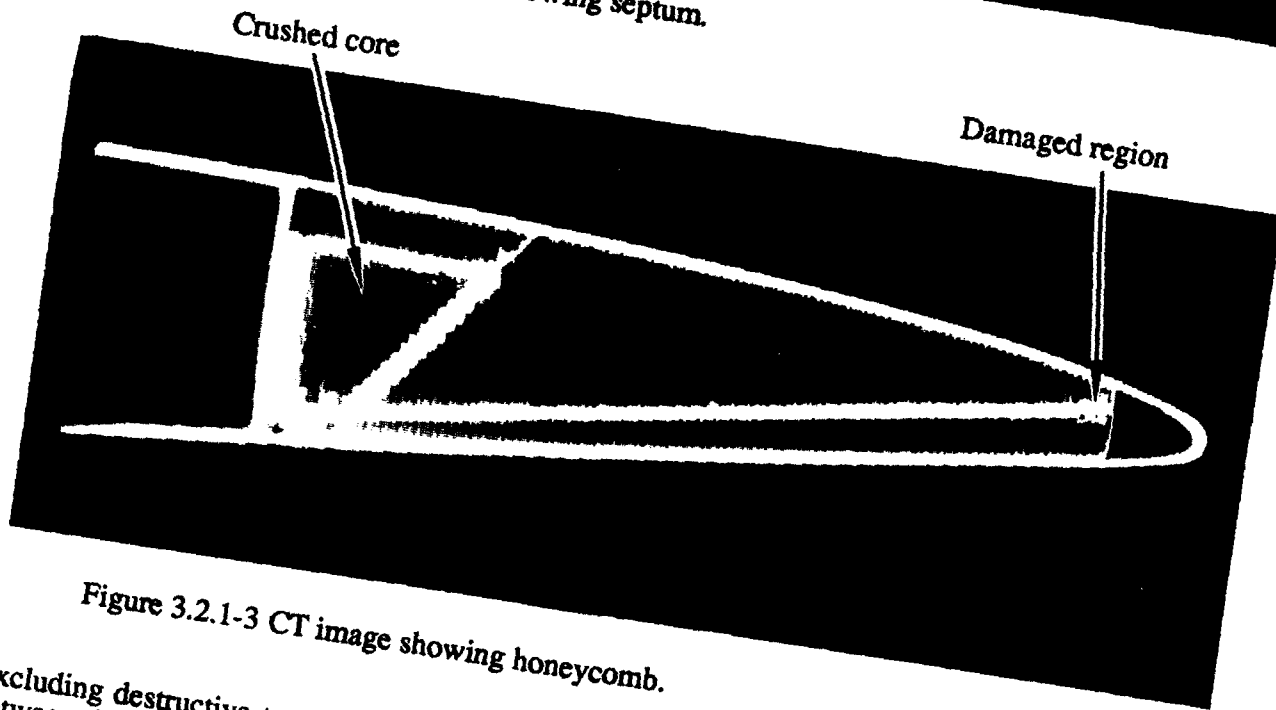


Figure 3.2.1-3 CT image showing honeycomb.

Excluding destructive testing, there is no other way to determine the condition of the bonding between the septa and the honeycomb, or of detecting or assessing other internal damage such as the crushed one.

Because this leading edge was a study prototype, it is impossible to estimate the total economic impact of CT to the development program. In addition to evaluation of prototypes, CT could just as easily be used for final manufacturing inspection, and subsequent maintenance inspections or "health checks." If knowledge of the internal materials is critical, then CT is essential for the successful completion of the program itself.

Another example of a honeycomb core composite with internal septa is the trailing edge made with a nomex core and a fiberglass/epoxy skin. A photograph of this rather large component (approximately 2.4 x 0.9 x 0.6 m (94 x 35 x 24 inches)) is shown in Figure 3.2.1-4. The trailing edge was made from several honeycomb sections, cut at angles to one another, and bonded together with a foaming adhesive. A good bond between cores, with minimal spreading of the adhesive, is important at these locations. An internal septum along the length was formed by bonding two halves together. This was done by placing a layer of prepreg cloth between layers of film adhesive bonded to each half.

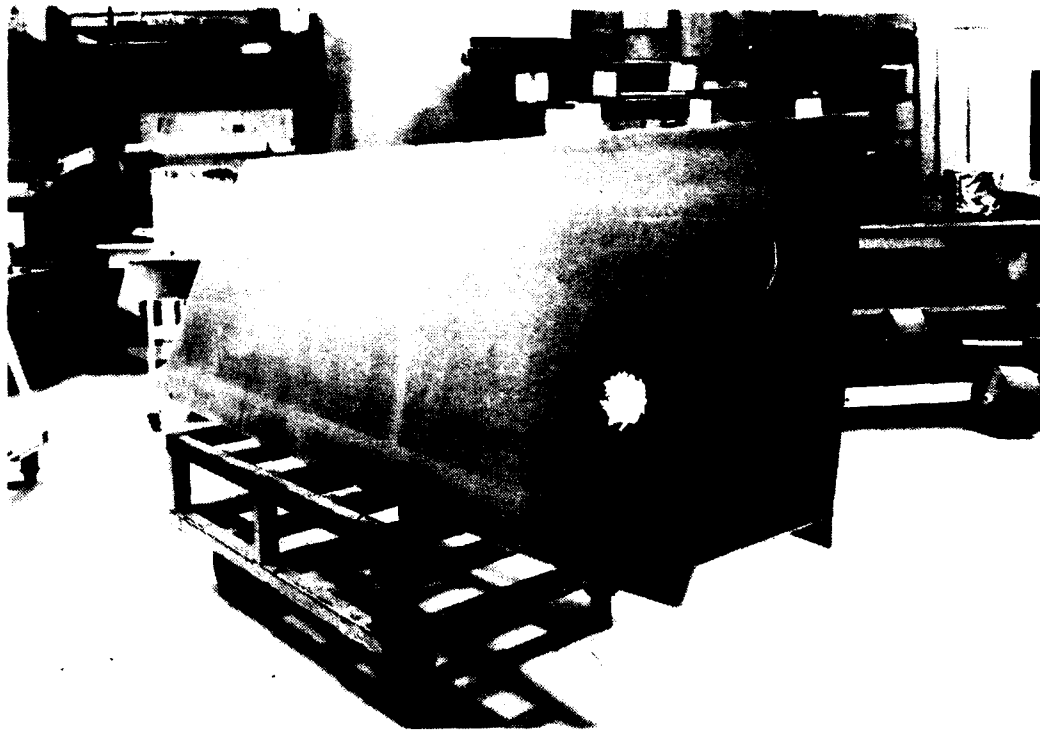


Figure 3.2.1-4 Photograph of a honeycomb trailing edge.

When a small vacuum is pulled on the part to assist skin-to-core bonding, the core tends to compress. This compression can form small delaminations along this bond because the prepreg does not contract, but rather tends to wrinkle. CT was used to evaluate this bondline, which was not inspectable any other way. CT slices were taken through the trailing edge at several locations along its length. The results of the CT scanning indicated that some wrinkling of the prepreg occurred at the internal septum, producing small delaminations at various locations along the bondline. Figure 3.2.1-5 is an example of one of the scans and Figure 3.2.1-6 is an enlargement of the bond line. The slight wrinkles along the septum are barely imaged. Because of the small size of the delaminations, a calibration standard with known defects would be necessary in order to actually quantify the relative amount of delamination across the entire bondline. Also seen in the image is the bond between two sections made with foaming adhesive, and the facesheet-core bond, which involved the bonding of both a film and foaming adhesive to the facesheet and core respectively before they were bonded together. CT was able to determine that these bonds were properly formed along the length of the composite. Figure 3.2.1-7 is a CT image at another location that is enlarged to maximize the detail at the bond line.

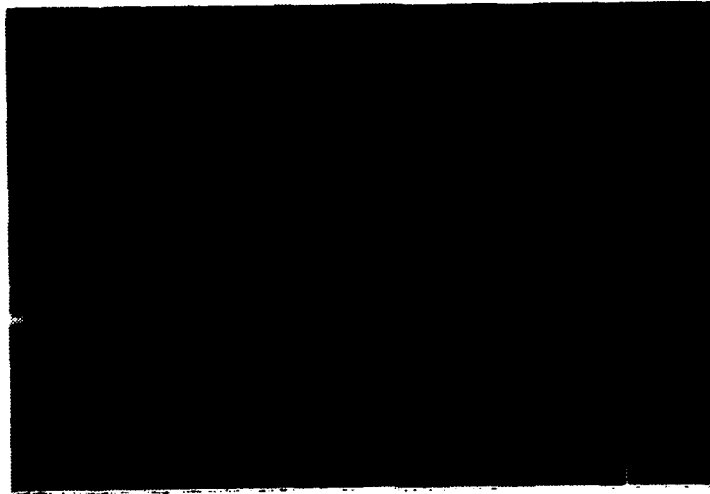


Figure 3.2.1-5 CT image of honeycomb trailing edge.

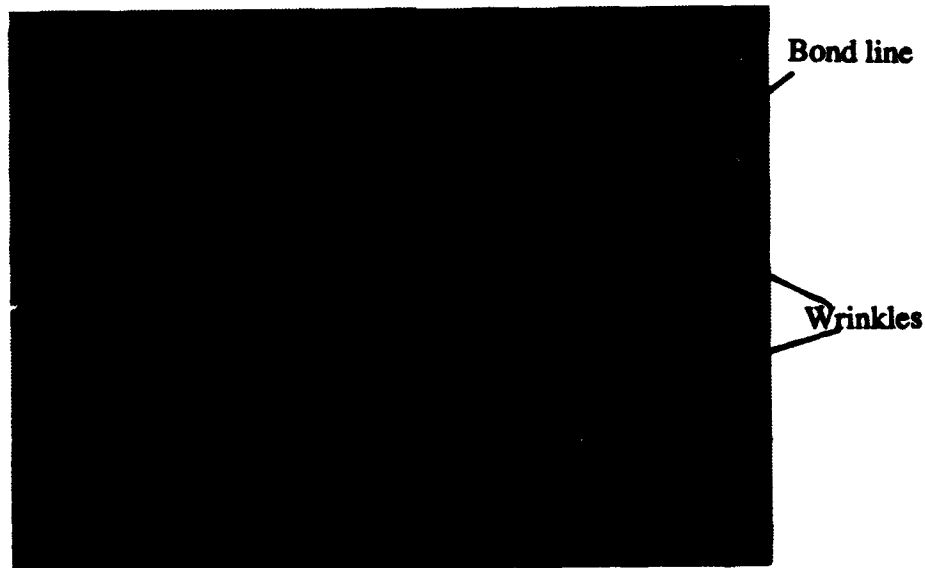


Figure 3.2.1-6 Enlargement of Figure 3.2.1-5 showing bond line.

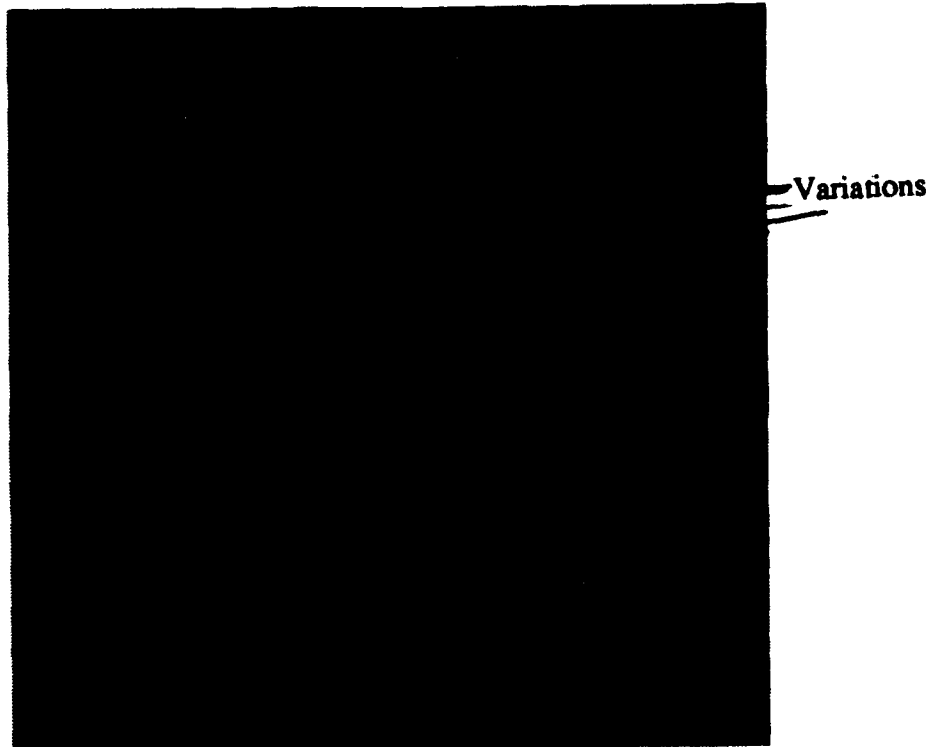


Figure 3.2.1-7 CT image showing variations along bond line.

These examples illustrate the effectiveness of CT for use in evaluating the internal configuration of complex honeycomb core composites, which cannot be adequately inspected by traditional nondestructive methods. The data can be used by engineers to evaluate modifications to the manufacturing process. CT should be an important tool for the development of new honeycomb structures.

3.2.2 Water Presence in Honeycomb Panels

During the manufacture of honeycomb panels, it is possible, as part of the process or in various handling steps, to have water enter and remain in the honeycomb. An example is the large graphite panel, approximately 2.2 m (86 inches) tall by 360 mm (14 inches) wide by 20 mm (0.8 inches) thick, shown mounted on a medium resolution CT system in Figure 3.2.2-1. While radiography can show the water is located in the panel, the radiograph can not tell how the water lies in the honeycomb cell. A CT image, like Figure 3.2.2-2, shows the distribution of water in the cell. Water is detected in three cells, but can be on either side of the structure. CT slices can be taken at locations of water presence, detected by digital radiography on the CT system, throughout the structure to measure the amount of water in the cell.



Figure 3.2.2-1 Photograph of long honeycomb panel mounted on a CT system.

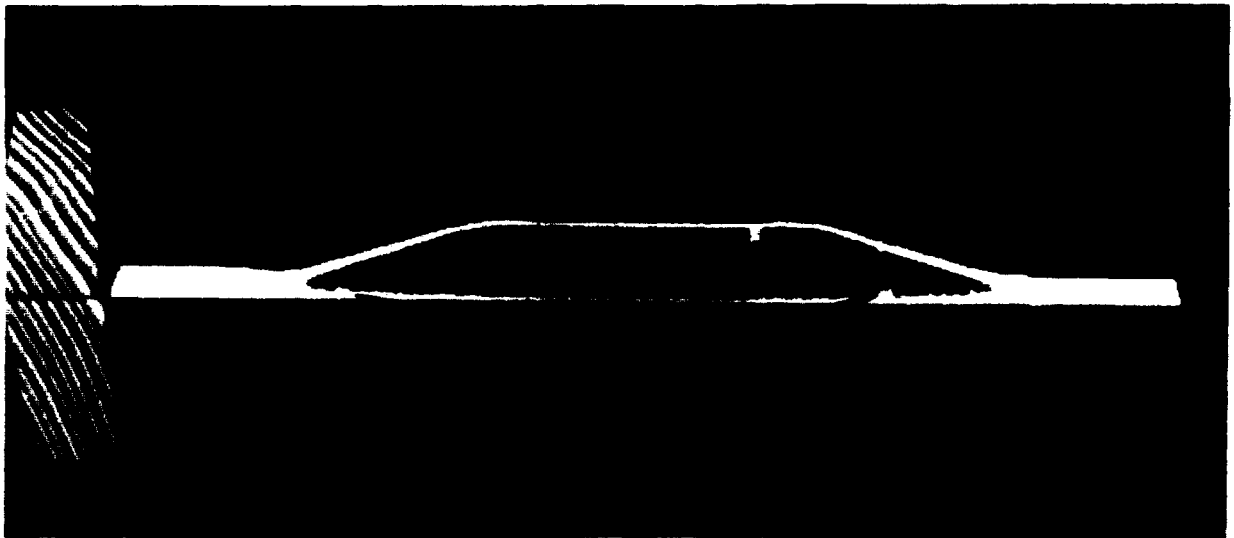


Figure 3.2.2-2 CT image showing water distribution in the honeycomb structure.

An analysis of the effect of the water was performed on test panels, using CT as a tool to measure the amount of water and movement of the water as a result of environmental tests. Two test panels, 400 x 360 mm (16 x 14 inches) in size, were fabricated with nomex honeycomb core and graphite epoxy skin, having a total thickness of about 20 mm (0.8 inches). One panel contained only the residual water that occurred in manufacturing, and the second panel was purposely injected with known amounts of water.

Digital radiographs (DRs) were made to determine the location of water. Then, CT scans were used to determine the distribution of the water in the plane normal to the radiography and to examine the condition of the honeycomb material and the bondline at the interface between the panel facesheets and the core. The panels were scanned prior to, midway through, and after thermal cycling.

The first series of DRs were taken with the panels mounted in a vertical plane to determine the locations where water was present. These DRs revealed that essentially no change in the water content of panel 1 occurred as a result of the thermal cycling. For panel 2, however, there was a different story. A DR of panel 2, taken before thermal cycling, is shown in Figure 3.2.2-3. Cells containing any significant amount of water are easy to detect in this figure. Figures 3.2.2-4 and 3.2.2-5 are DRs of the same panel taken midway through and after the thermal cycling, respectively. It is clear that the water in column 2, row 4, and column 4, row 3, is migrating as the panel experiences thermal cycling.

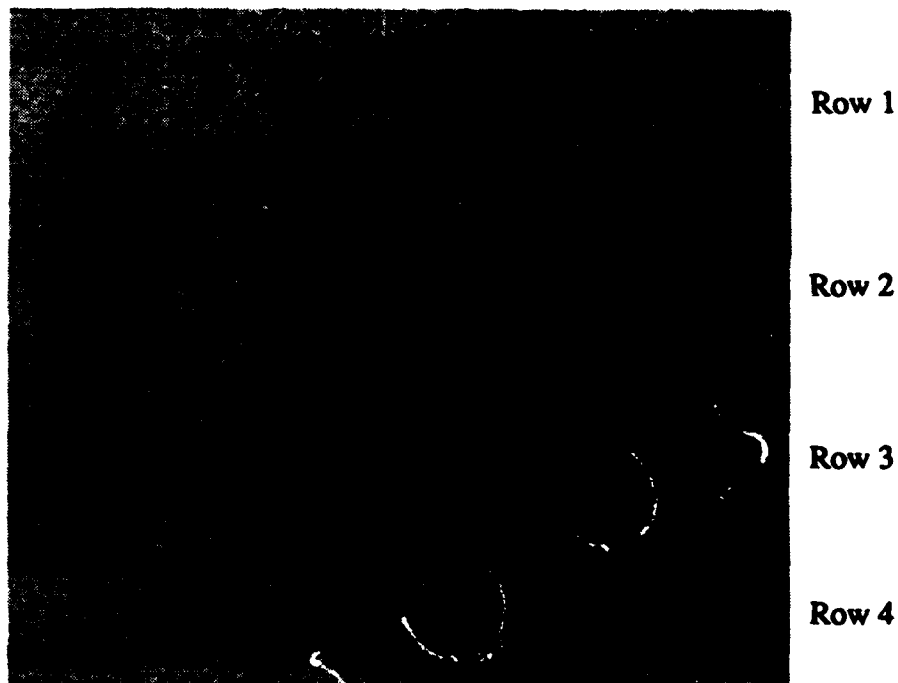


Figure 3.2.2-3 DR image showing water distribution in test panel prior to environmental cycling.

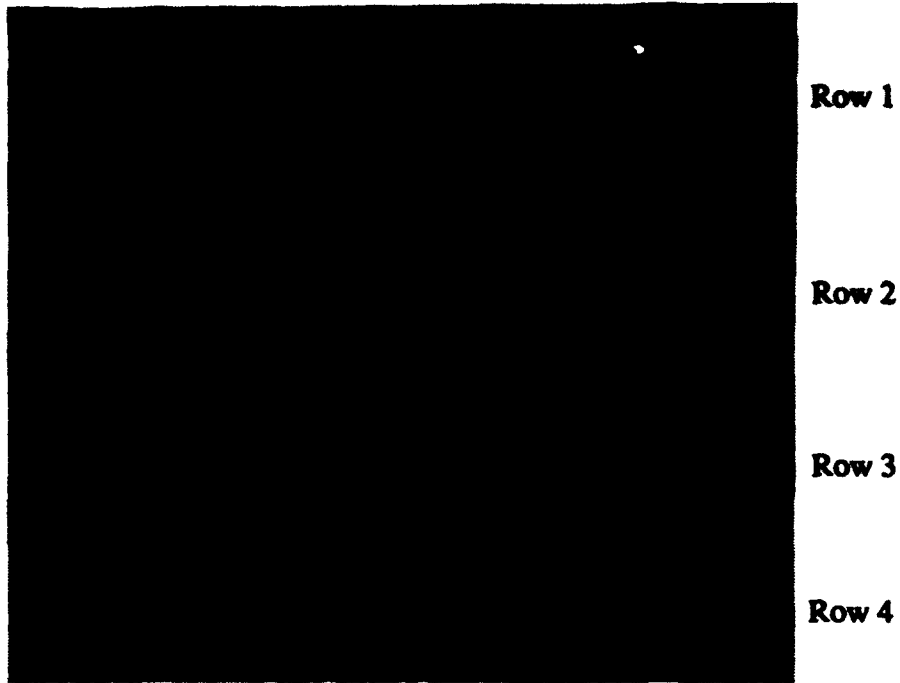


Figure 3.2.2-4 DR image showing water distribution in test panel midway through environmental cycling.

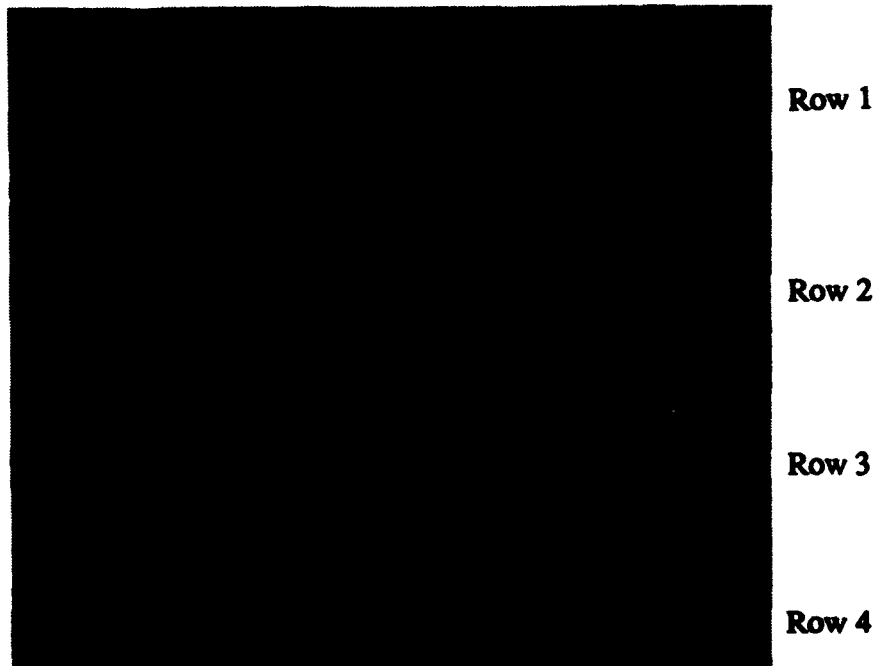


Figure 3.2.2-5 DR image showing water distribution in test panel after environmental cycling.

A series of CT slices were taken with the panels mounted in the horizontal position to quantify the amount of water in the panels by obtaining a volume data set. By orienting the panels horizontally, the number of CT slices to cover the 20-mm-thick panel is minimized. These slices were taken both before and after the thermal cycling. The data was processed to threshold the water in each CT slice, creating contours which define the location of the water. The area of the image contours was calculated for each slice. Since the number of slices and their spacing are known, the total volume of water can be calculated. The CT slices taken near the top and bottom of the series were partially volumed by the panel sheets and the adhesive of the honeycomb. For panel 2, the volume of water was determined to be 4.8 cm³ pre- and 4.4 cm³ post-environmental test. The pretest value was very close to the estimate of the injected quantity of water. Because the water was migrating under the environmental test, some of the water ended up in cells at such a low level that it was impossible to distinguish from the interference with the adhesive layer bonding the honeycomb to the panel substrate, resulting in a lower volume measurement in the postcondition. Figures 3.2.2-6 and 3.2.2-7 are slices taken in panel 2 in the pre- and post-conditions, respectively. Figure 3.2.2-6 is a slice taken at approximately 1.5 mm (0.06 inches) above the bottom of the panel, and Figure 3.2.2-7 is a slice taken at approximately 2 mm (0.08 inches) above the bottom. It is again easy to see the net migration of the water.

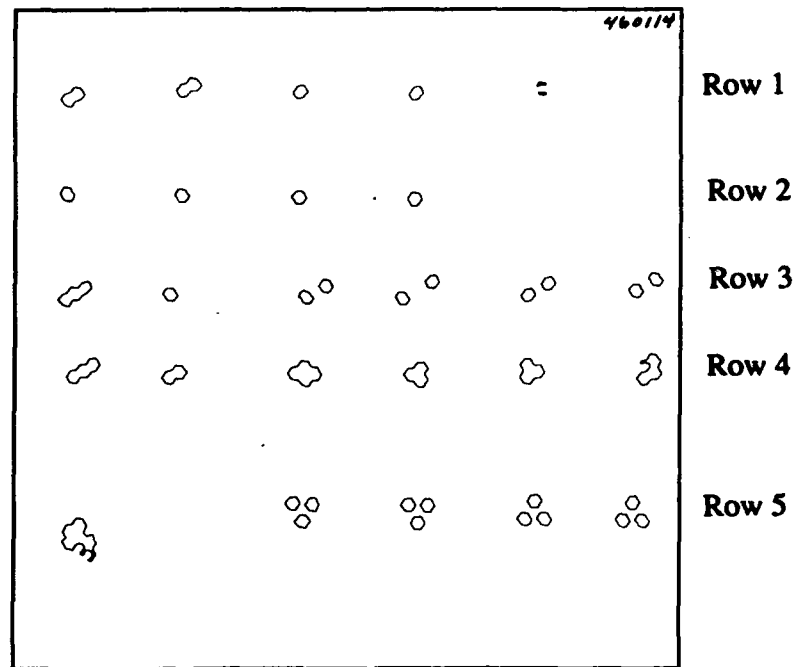


Figure 3.2.2-6 CT image of panel 2 showing water distribution in cells at 1.5 mm (0.06 inches) above the bottom preenvironmental cycling test.

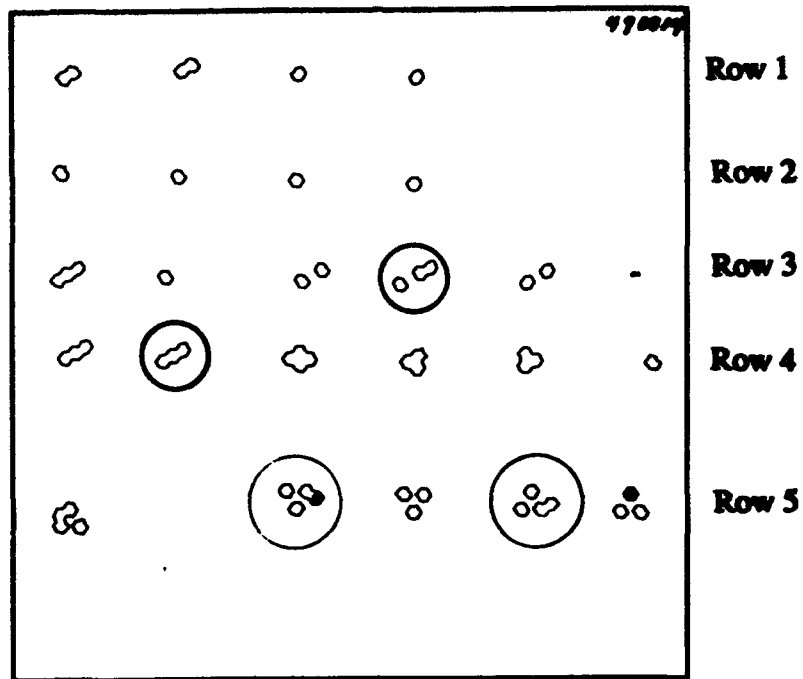


Figure 3.2.2-7 CT image of panel 2 showing water distribution in cells at 2 mm (0.08 inches) above the bottom postenvironmental cycling test.

The observed migration in panel 2 could possibly be attributed to a leak caused by the drilling process used to inject water for the thermal cycling test. A CT slice taken with panel 2 in the vertical position appears in Figure 3.2.2-8. It indicates a damaged cell, which is in the column 4, row 3 water containing cell cluster of Figure 3.2.2-7.

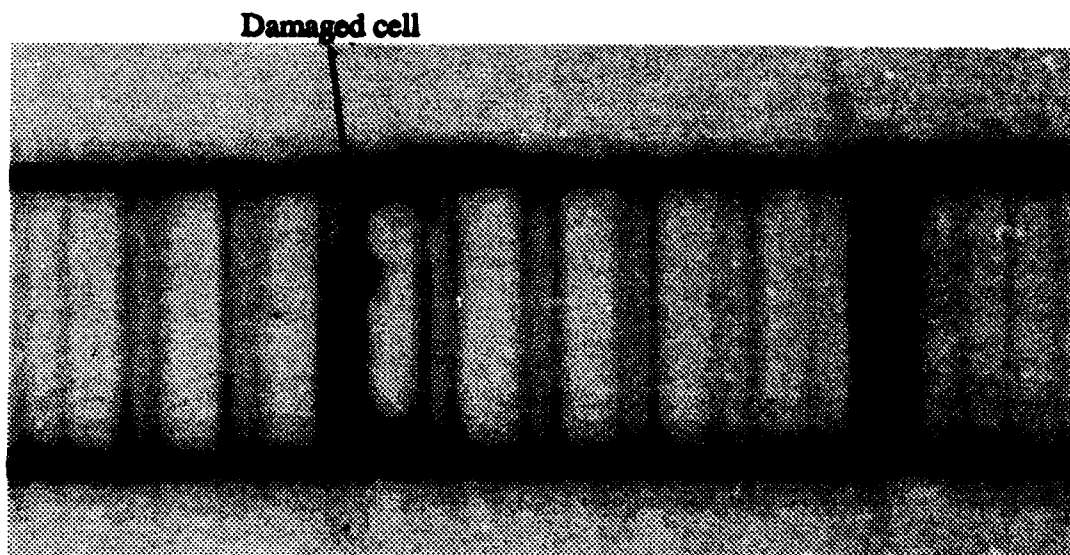


Figure 3.2.2-8 CT image across cells of panel 2 showing damaged cell.

In addition to quantifying the amount of water in the panels and showing how the water is redistributed as a result of thermal cycling, CT made it possible to inspect the condition of the honeycomb cell walls and the face sheet/core bondline. The core condition was generally very good, with the possible exception of drill damage, and there were no disbonds along the bondline. This information allowed engineering to make appropriate recommendations for the disposition of panels. No other nondestructive inspection method could have provided the quantitative information on the volume of internal free water trapped in the honeycomb core. Without CT, destructive testing would have been required for the water volume determination. This would have required more samples and there would have been a much greater risk of misunderstanding because measurements could not be made pre-, mid- and post-environmental testing on the same panel. For a test program, CT can provide considerable savings in the number of samples by providing better measurements on fewer samples than alternative approaches require.

3.2.3 Honeycomb Panel with Internal Features

Honeycomb structures will often be inspected by large area NDI techniques. Test specimens must be fabricated to establish the sensitivity of the NDI method. CT can provide information on the test specimens to show that they are fabricated correctly, with suitable features for the NDI evaluation. A photograph of a test panel is shown in Figure 3.2.3-1. The panel is approximately 600 mm (24 inches) square and 50 mm (2 inches) thick. The aluminum core has sections of three different densities and is comprised of sections of two differing thicknesses. The panel contains a number of features intentionally engineered into the honeycomb interior, allowing it to be used as a standard for thermographic NDI. These features include depressions machined into both of the surfaces of the aluminum core, crushed portions of core material, various types of adhesives between the core and the panel skins, and several repair regions.

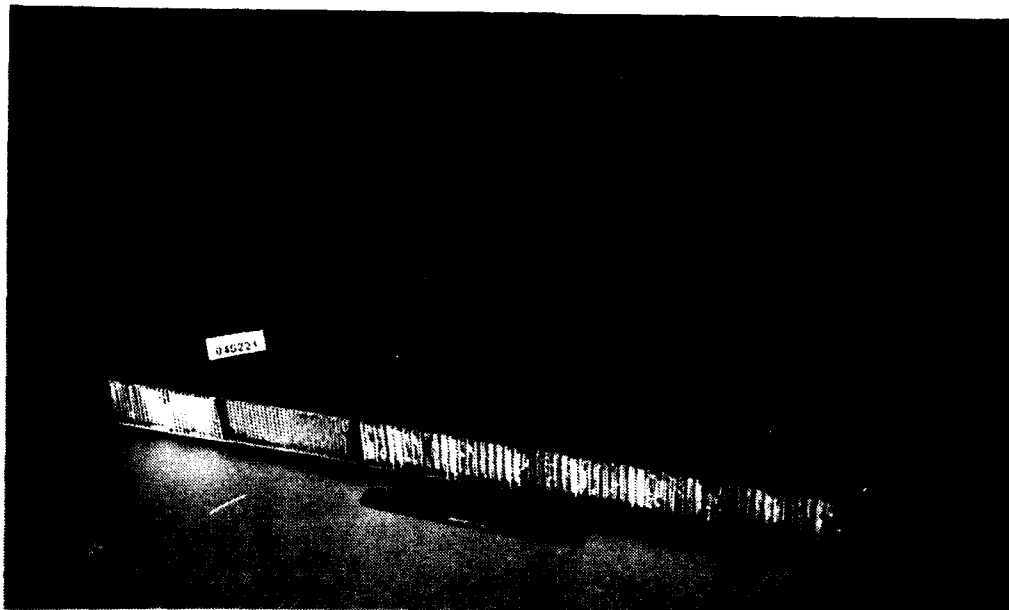


Figure 3.2.3-1 Photograph of a composite test panel.

The skins of the panel were fabricated with some areas having a different number of plies than others. All told, there were areas of 3, 9, 13, and 36 plies on one skin, and 4, and 10 plies on the other. One of the composite skins was cured first, and then bonded to the aluminum honeycomb core, and the other was laid up on top of the core and then cured.

Five different CT slices of the panel were taken. The object of the various slices was to confirm the extent and distribution of foaming adhesives, the condition of other types of adhesives, the porosity of the composite skins, and the general condition of the features inside the panel.

An image of one CT slice is shown in Figure 3.2.3-2. The upper skin in this figure contains a portion of 36 plies on the left-hand end. In roughly the center of the upper skin, there is a pocket machined into the honeycomb core. An adhesive layer is seen to be sagging slightly into this layer. The core itself is least dense, 0.24 g/cm^3 (3.1 lb/ft^3) over the left hand two thirds, then a section which is more dense, 0.47 g/cm^3 (6.1 lb/ft^3) over approximately the next sixth, and finally a section which is much more dense, 1.7 g/cm^3 (22.1 lb/ft^3) of the same width appears on the right. The medium density section is slightly less thick, as can be evidenced by observing the depression in the upper skin covering that portion of the panel. The upper skin was laid up and cured on the core. At four places along the bottom, just above the skin, foaming adhesive is seen. This adhesive was introduced into four "pockets" machined into the lower surface of the various sections of the core.

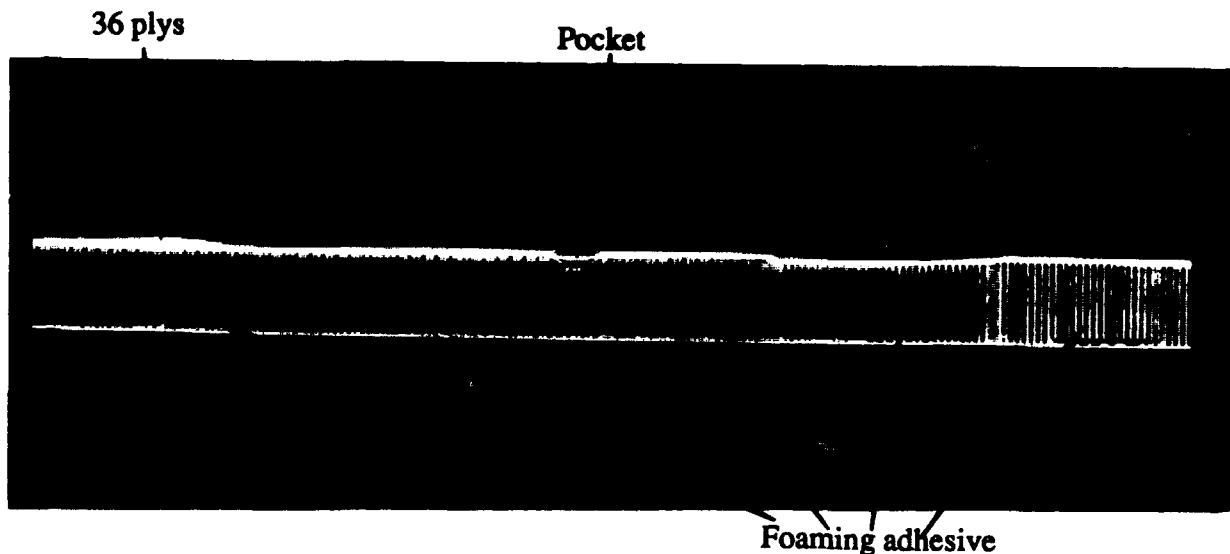


Figure 3.2.3-2 CT image of panel.

Figure 3.2.3-3 is an image of a slice taken parallel to that of Figure 3.2.3-2, but closer to the edge of the panel section. The three different core densities are again displayed, along with several other important features. Along the upper interface between the core and the skin there are two instances where sections of the skin have "sagged" into "pockets" machined into the upper surface of the core. These are at the extreme left, and again in approximately the center of the figure. At the left end of the figure, the 36-ply-thick upper skin is seen to taper down to the 13 plies proceeding from left to right along the top of the panel. This section also contains some porosity. Also, on the bottom left side, there is a 10-ply section that goes somewhat further than the 36-ply section on the top; but this section comes to an abrupt edge, becoming 4 ply as per design. Just above this section, there is some noticeable adhesive.

Porosity

Sagging



10-ply section

Figure 3.2.3-3 CT image parallel to Figure 3.2.3-2.

Figure 3.2.3-4 is an image of another CT slice taken about 75 mm (3 inches) away from the CT slice shown in Figure 3.2.3-2, but skewed slightly relative to the panel edge. This figure shows nine "pockets" machined into the upper surface of the various honeycomb sections. The dimensions of these pockets can be easily confirmed as per drawing. Also, there are four pockets similar to those on the lower surface of Figure 3.2.3-2, but in this case, there is no foaming adhesive. Those pockets in the light density core area (the left-hand two-thirds of the panel) are more difficult to see than those in the medium and high-density areas because the density difference in these latter two areas is greater.

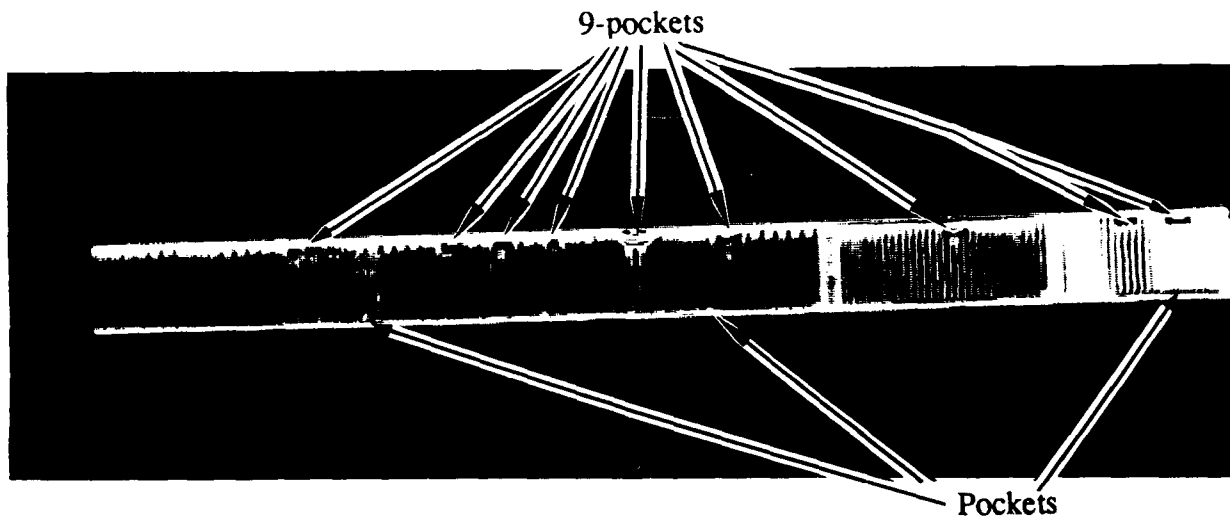


Figure 3.2.3-4 CT image of panel.

Figure 3.2.3-5 is an image of a CT slice taken across the panel perpendicular to the CT slices in Figures 3.2.3-2 through 3.2.3-4, cutting through the region containing only the light density core material. In several places, foaming adhesive is evident. The upper skin has sections of 36 plies on the left, tapering to 9 plies in the center, and finally to 3 plies on the right. The lower skin starts at 10 plies on the left then tapers to 4 plies for the remainder of the panel. Adhesive curling is seen on the bottom skin/core interface near the left end of the panel. Careful observation of the image on the CT system monitor showed some porosity in the 36-ply section on the upper left.



Figure 3.2.3-5 CT image across panel.

This panel provided a variety of features to inspect and is a good example of the versatility of CT to evaluate the, otherwise, inaccessible interior of complex composite parts, which can be made of a variety of materials. Although all of the various features of interest were not discussed above, CT provided necessary and useful information for the following: 1) how the film adhesive contacts and wicks down the honeycomb, 2) sagging of unsupported film adhesives or skin plies, 3) whether core splices are properly filled with foaming adhesive, 4) porosity in the thick-skin area, 5) extent of migration of both foaming adhesive and the epoxy used for repairs, and 6) the shape of pockets machined into the honeycomb core. In this example, CT proved to be valuable by verifying that the features designed into this complex NDT standard panel were built as planned. CT provided views of the interior structure which cannot be provided by any other NDT technique.

3.3 Difficult/Complex Structure

The use of complex or difficult to measure geometries is important to emerging aerospace materials and processes for high-performance aircraft structures. CT can be a useful tool to assist the development of these products.

3.3.1 Graphite/BMI "V" Section

The aft boom fairing on the F-22 ties the vertical tail into the upper aft skin and is an example of developing a difficult-to-manufacture geometry. As part of the subscale testing of the chosen concept, layup of the graphite/BMI over a tight radius (0.5 mm (0.02 inches)) was required. Several parts were fabricated for the purpose of determining if the tight radius could be made while maintaining a good quality part. Figure 3.3.1-1 is a photograph of a test piece. While UT was sufficient for evaluating the flat areas of the parts, the very tight radius could not be adequately evaluated with this or any other conventional NDE method. CT was successfully used for examining the material at the radius of several parts.

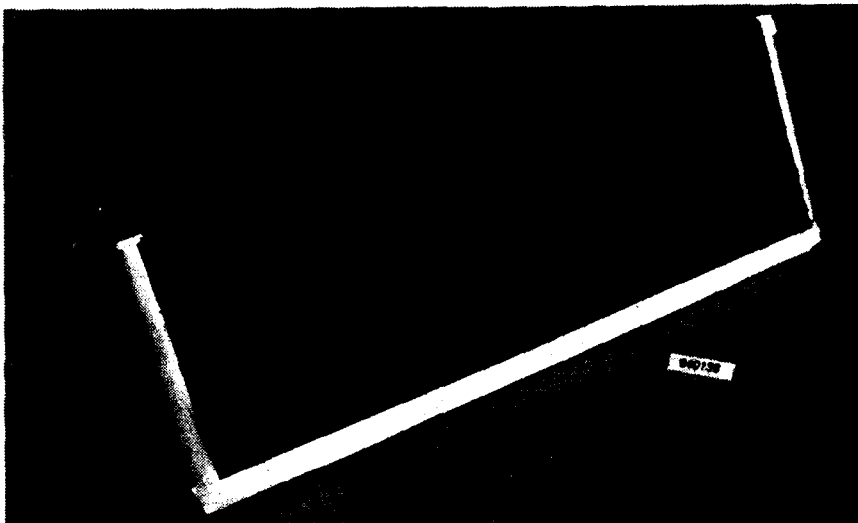


Figure 3.3.1-1 Photograph of "V" shaped composite test panel.

CT slices of structures that have straight sections will have streak artifacts that tend to obscure the regions of interest, such as the root radius of the "V" section. Figure 3.3.1-2 is a typical image containing artifacts at the "V" section root. Artifacts can be reduced through the use of bolus or filler material, which is packed inside and/or around the part to be scanned, thereby reducing the density differences at the part edges. In this case, it was found that a bolus (fine, white sand) that was slightly more dense than the composite virtually eliminated the artifacts at the root radius, and allowed CT measurement of the material consolidation of the region.

Figures 3.3.1-3 and 3.3.1-4 are example images of the "V" section with the sand bolus filling the interior. At the root radius of the "V" the material consolidation is evaluated. Figure 3.3.1-3 is an image from the first article and Figure 3.3.1-4 is an image from the second article showing improvement to the process.

A quantitative measurement of the consolidation of the composite at the root radius could be made by examining the CT data. The mean CT value in a region can be correlated to the actual material density, while the standard deviation provides a measure of the uniformity of the

composite in that region. A circular region of interest whose diameter was half the thickness of the part was chosen for statistical comparisons at several different locations, as indicated in Figure 3.3.1-5. The result of the CT measurements are given in Figure 3.3.1-5 at locations A, B, and C for two "V" sections examined with CT.

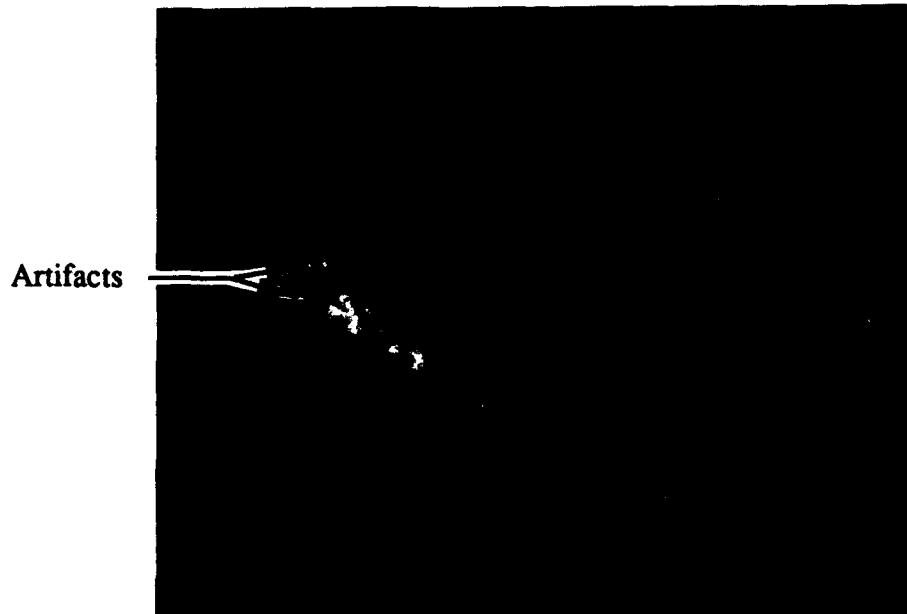


Figure 3.3.1-2 CT image of "V" section showing artifacts.

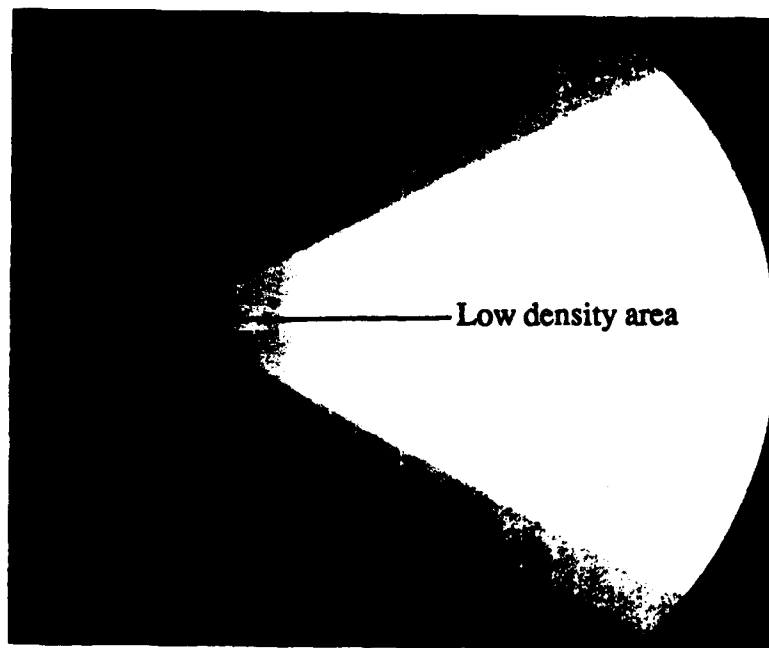


Figure 3.3.1-3 CT image of "V" section using bolus to reduce artifacts for article 1.



Figure 3.3.1-4 CT image of "V" section for article 2.

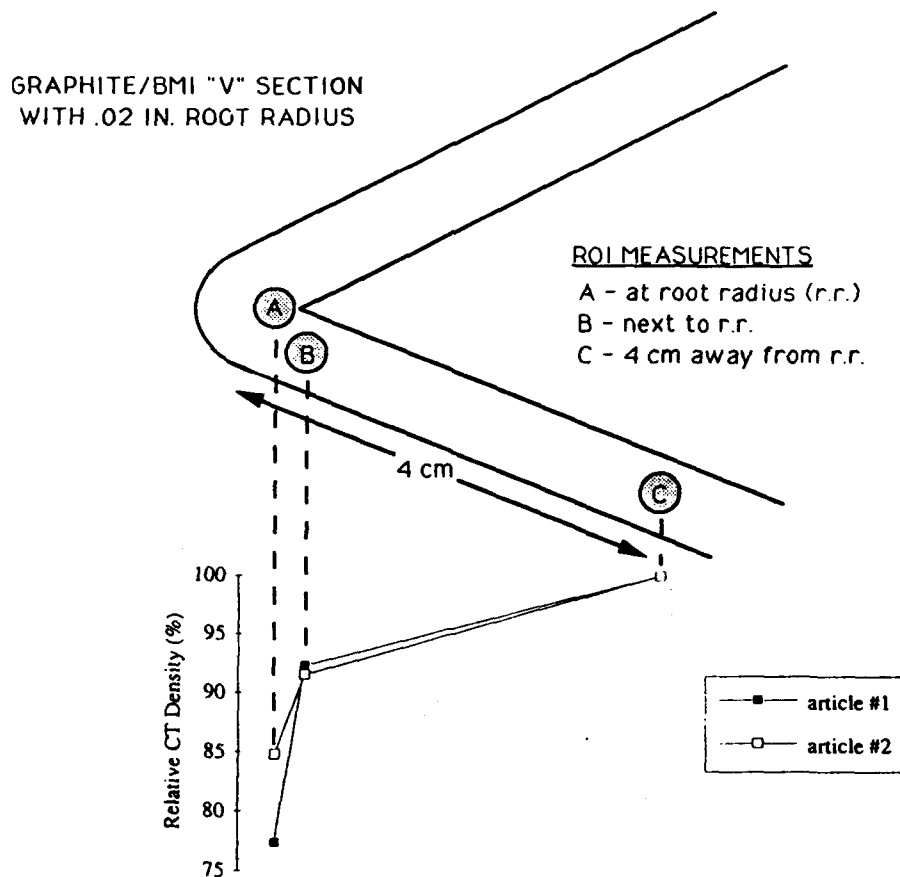


Figure 3.3.1-5 Drawing showing region of interest and CT measurement results.

Several conclusions can be drawn from these results. First, the material density at the radius is slightly lower than the flat regions, but there are no major voids or significant resin starved areas. Second, the material density is slightly less uniform in the radius region, but the difference is not significant. Third, there was an improvement in the density level and uniformity between the first and second "V" section. The CT results were useful in verifying that the chosen material system could be successfully laid up over the required radius. The information from these tests was used to establish the design of the tool for fabricating the composite fairing. CT proved to be invaluable on this program. The engineer responsible for demonstrating the concept stated that CT was the only NDE method they had found that actually allowed them to examine the material quality of the radius.

3.3.2 Sinewave Spar

A variety of spar geometries are used on aircraft skins to provide added stiffness and strength. Sinewave spars - spars with sinusoidal shaped webs - have a particularly good stiffness-to-weight ratio, and will replace conventional straight web concepts on new advanced aircraft such as the F-22. Because of their complex geometry, however, sinewave spars are more difficult to inspect. Ultrasonic testing, the standard NDE method for composite spars, requires curve-following or multiple-angled scanning to properly inspect the web for delaminations, voids, and other defects. Because the flanges are basically flat, they are easily inspected with UT from the cap side, but the critical web/flange intersection is not fully characterized from that side. UT scanning that follows the radius of the intersection is required. Not only is this complicated, but the interpretation of the data is difficult.

While it may not replace UT for general inspection of sinewave spars, CT appears to have potential as an evaluation tool for the web/flange intersections. An earlier CTAD report on CT for composites indicated just that [4]. In order to assess the defect detection capabilities of CT at these intersections, a thermoplastic sinewave spar was evaluated on a medium resolution CT system. Figure 3.3.2-1 is a photograph of a section of a spar. Previous CT scanning with a medical system had indicated that flaws were present in critical areas [4], but the resolution of the medical CT images was not sufficient to actually characterize the defects.

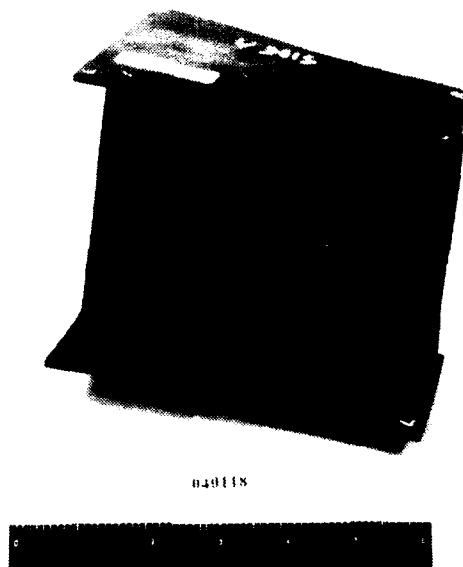


Figure 3.3.2-1 Photograph of a test section of a sinewave spar.

The spar was placed in a container of fine grain white sand to eliminate the streak artifacts that are produced along long straight path lengths in CT images. For a spar with an "T" beam CT cross section, these artifacts would cross at the web/flange intersection and tend to obscure the data. The sand bolus was very effective, and virtually eliminated the artifacts. A series of CT slices were taken at 400 kV and 2.3 mA with 2-cm-slice spacing along the spar section. Figure 3.3.2-2 is a typical CT slice.

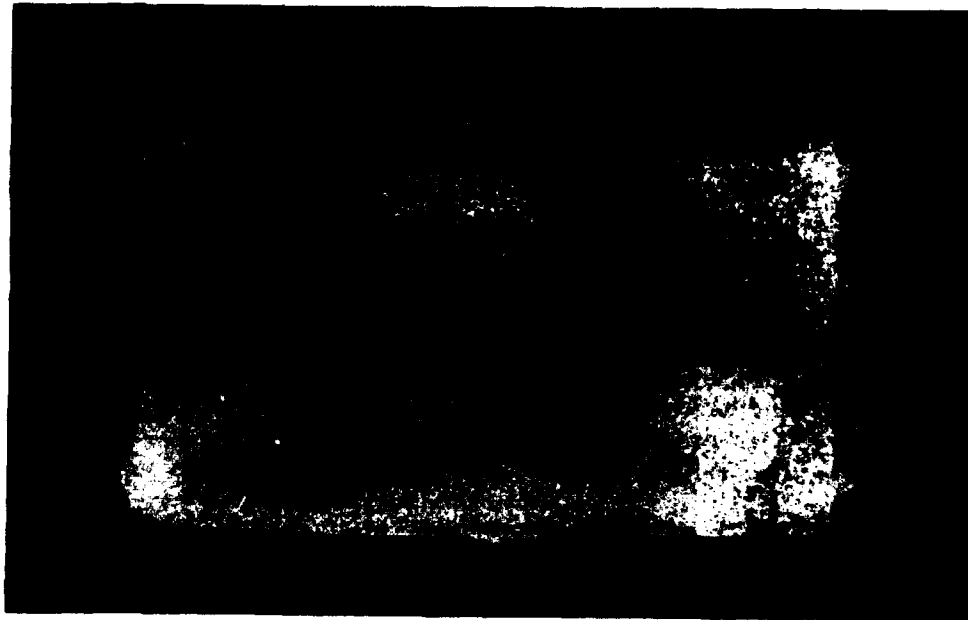


Figure 3.3.2-2 CT image of a sinewave spar.

Delaminations and cracks that connect delaminations were found near one end of the spar section at the web/flange intersections. A series of contiguous slices were then taken in this region in order to more fully characterize the flaws. Thirty-one slices 1 mm (0.04 inches) apart were taken over a 3-cm (1.2 inch) length to produce a 3-D data set of the area. Part of the series of slices (every fourth image) is shown in Figure 3.3.2-3, where the right web/flange intersection is isolated. The shape, size, and relative location of the cracks and delaminations are clearly defined within the spar cross section.

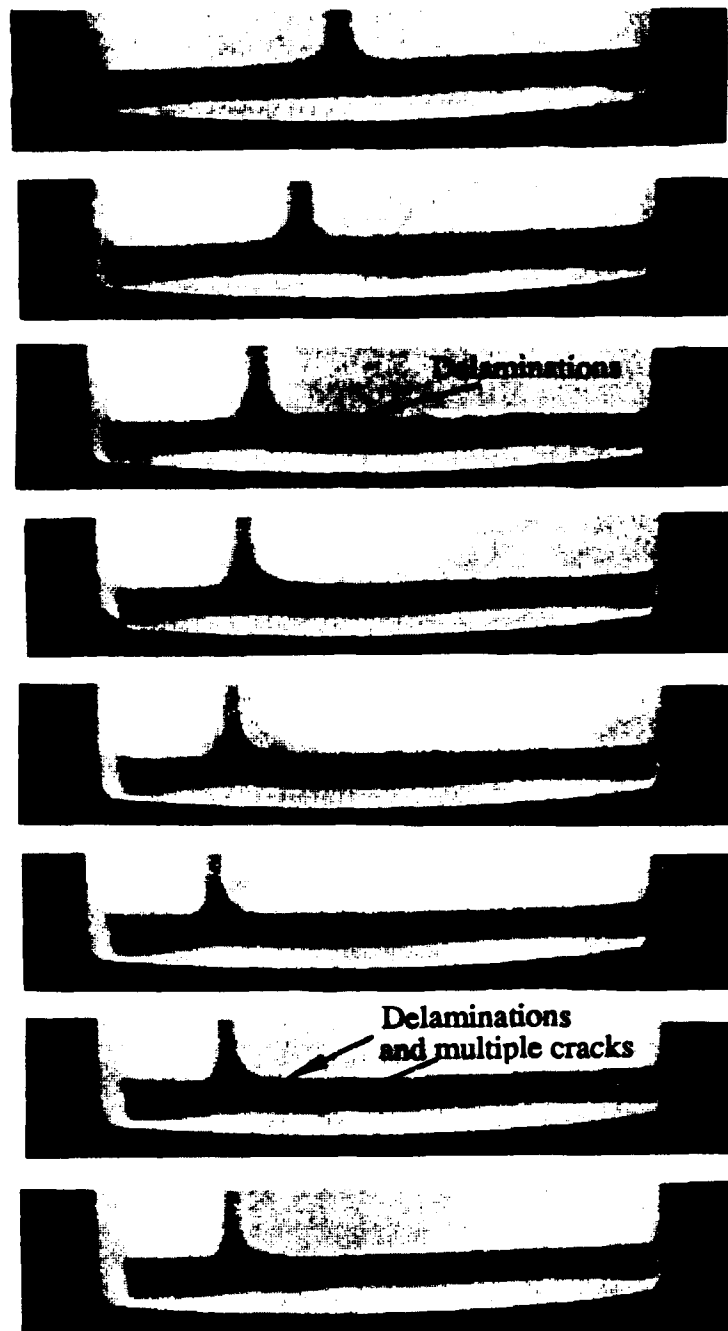


Figure 3.3.2-3 CT image series of a sinewave spar showing flange cracks and delaminations.

The defects in this spar are relatively large. Not all cracks or delaminations that must be identified will be this significant. However, it is clear from the definition in these scans that smaller defects can be imaged. The CT data provides spatial characterization of the flaws, which can be used to make informed decisions about needed process modifications, and to predict part performance. At the same time, the CT data can provide a complete dimensional measure of the spar at any chosen location. If CT were to be used as a defect detection tool for the web/flange intersections, required dimensional measurements could be made simultaneously and

automatically using software designed for this purpose. A system that takes slices as the part is passed through it horizontally could be designed and built for this specific application. CT scanning could initially be done at specific regular stations, and extra slices could be made at regions of concern or where potential flaws are indicated by digital radiography or ultrasonics. For the best possible data, bolus material may be required. The bolus could be in solid or liquid form, adapted to the particular application for ease of implementation.

The development of a CT system for evaluating sinewave spars appears to have considerable merit. It would be worth pursuing this approach with a small trade-off study that examines the costs and effectiveness of the various NDE methods available for sinewave spars.

3.4 Tows and Windings

Composite structures use fibers in a resin matrix for high strength along the fiber axis. The manufacture of these structures relies on the orientation of fibers and their uniformity to achieve the design goals.

3.4.1 Thick Composite Beam

A section of a solid composite beam is an example of using CT to evaluate the fiber/matrix condition with special interest in the extent of fiber-bundle waviness inside the beam. A photograph of the section of the beam is shown in Figure 3.4.1-1. The beam is 200 mm (8 inches) across and about 30 mm (1.2 inches) thick. The test section shown in the figure is only 84 mm (3.3 inches) long and has three holes (3, 5, and 7 mm (0.1, 0.2, and 0.28 inch) diameter) whose axes are perpendicular to the fiber plies making up the composite. The two outside thirds of the section were slightly thicker than the central third.

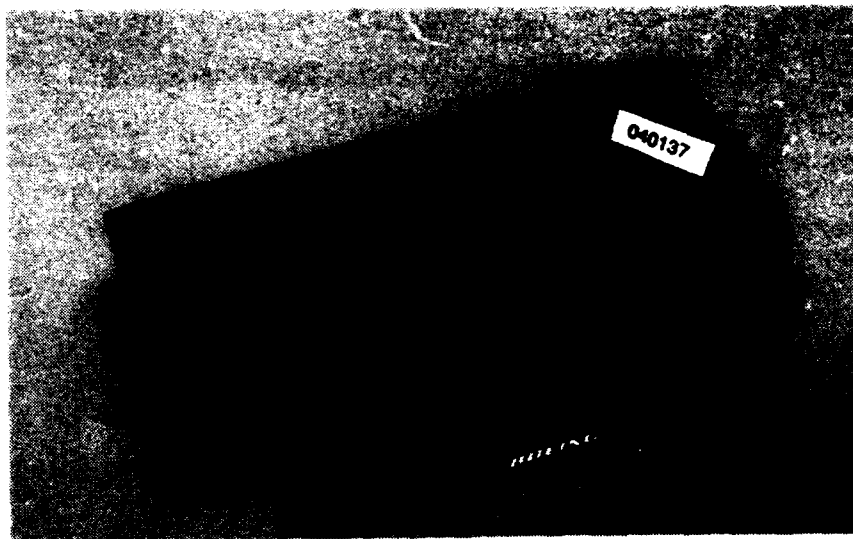


Figure 3.4.1-1 Photograph of a composite beam.

The test section was scanned with several slices taken at various locations along the length. A CT slice is shown in Figure 3.4.1-2. This slice is near the center of the section, showing the three holes. The beam is intentionally skewed along its length, making the CT image a parallelogram. The image easily resolves the various plies in the beam.

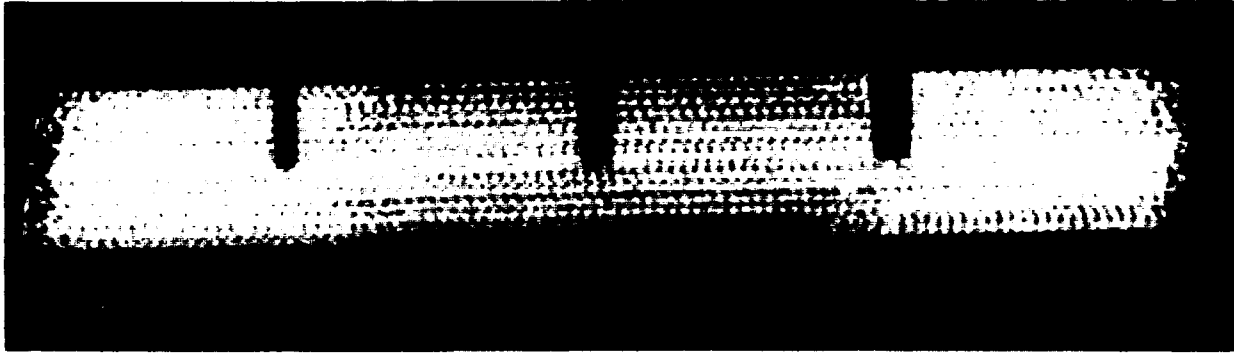


Figure 3.4.1-2 CT image of the composite beam.

In order to study fiber features in the individual plies, 20 contiguous slices were taken centered approximately over the middle of the beam section. From these slices, which comprise a three-dimensional data set, a multiplanar reconstruction (MPR) was performed. The software used in the MPR allows the isolation of perpendicular planes contained in the three-dimensional volume bounded by the data set. The planes parallel to the plies were chosen for evaluation of the beam. The software used in the reconstruction interpolates between slices across the 25-mm- (1-inch-) thick beam section. A wealth of information was revealed from inspection of the reconstructed planar sections.

Figure 3.4.1-3 is a reconstructed planar image at approximately 3.9 mm (0.15 inch) below the top surface containing the holes. Several features are noteworthy in this figure. First, the center section (approximately the central one third) appears to be resin starved compared to the two ends. This is indicated by the darker region occupying most of the center of the figure. The displayed portion of the reconstructed "slice" does not go the whole length of the beam, so this darker portion is more than a third of the figure length. The fibers, having the higher density, show up as lighter in these figures. Next, there is a fiber tow (bundle) in the right-hand portion of the figure which is out of alignment. This is the white line running diagonally up towards the end of the figure starting at the bottom just to the right of the large hole. It is generally very useful in the manufacture of composites to know if the fibers in a particular ply are properly aligned. In this instance, CT had no problem seeing fiber tows that were out of alignment.

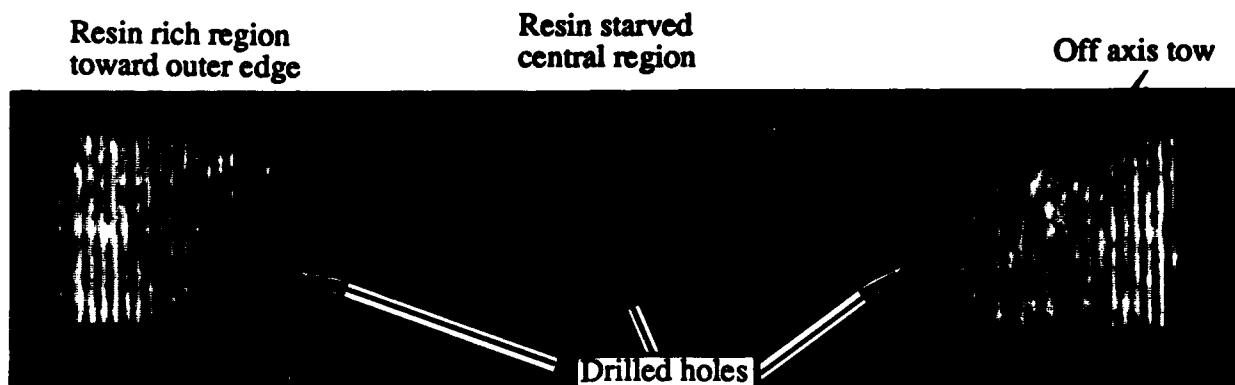


Figure 3.4.1-3 MPR reconstructed CT image of the composite beam at 3.9 mm (0.15 inch) from surface.

The main feature of interest in the investigation was fiber tow waviness. It turned out that some of the plies demonstrated a great deal of waviness in the fiber tows, while other plies contained fiber tows that appeared to be quite straight. Figure 3.4.1-4 is a reconstructed "slice" located approximately 10.8 mm (0.43 inch) from the surface of the beam section. The fiber tows appear to be quite straight for this particular ply. Figure 3.4.1-5 is a reconstruction of a "slice" located approximately 4.1 mm (0.16 inch) from the surface. In this case the fiber tows exhibit strong waviness, with a periodicity that appears to be roughly the same over most of the region of the ply bounded by the holes. There were several plies that exhibited this type of waviness, and several that had straight fiber tows.

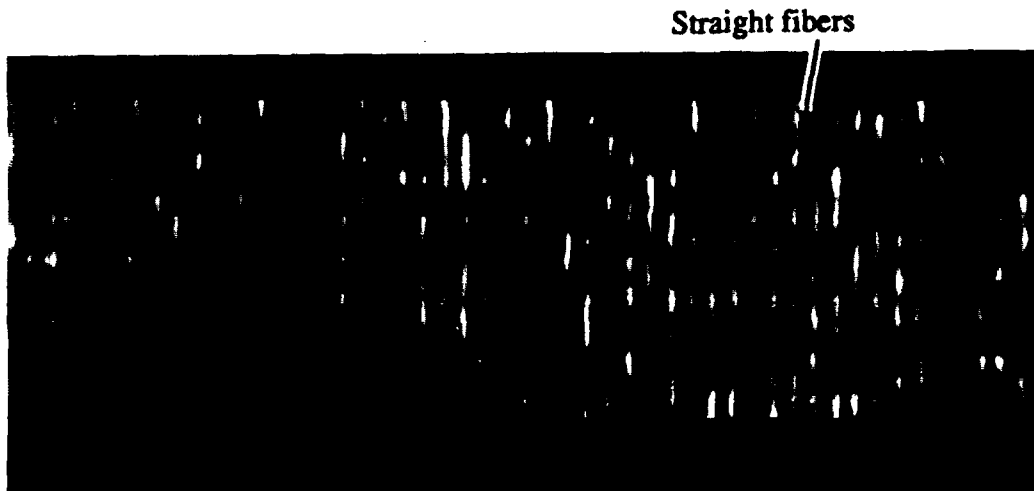


Figure 3.4.1-4 MPR reconstructed CT image of the composite beam at 10.8 mm (0.43 inch) from surface.

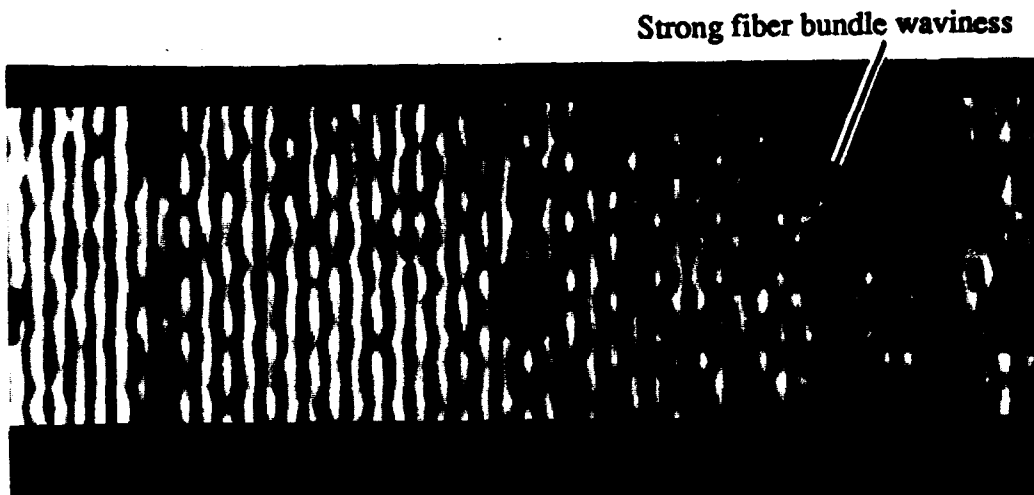


Figure 3.4.1-5 MPR reconstructed CT image of the composite beam at 4.1 mm (0.16 inch) from surface.

Finally, wrinkling in individual plies was also detected. Figure 3.4.1-6 shows some out-of-plane wrinkling in a ply located approximately 9.4 mm (0.37 inches) from the surface. The wrinkle goes roughly along the long dimension of the beam section. Starting at the left side of the image, it runs up to the top, then back down, and then horizontally through the center hole, then continuing slightly downwards as it runs horizontally to the right, apparently stopping at the largest hole. It appears as the part of the image that seems to be "out of focus"; this is because the tows in the wrinkled portion are not entirely contained in the reconstructed plane.

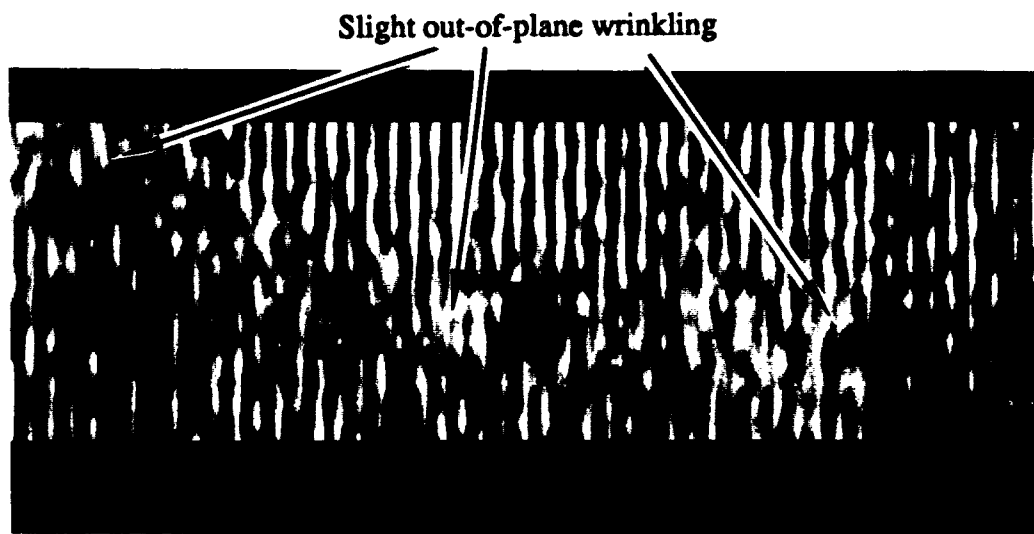


Figure 3.4.1-6 MPR reconstructed CT image of the composite beam at 9.4 mm (0.37 inches) from surface.

In the case of this solid beam section, CT has proven to give detailed information in fiber tow and fiber ply features. This type of information is available fairly routinely, as the system used to scan the section was a medium resolution system. The capability to do the multiplanar reconstruction greatly enriches the quality of the information concluded from scanning the article with a modest number of slices, (say 20 to 25), since it permits evaluation of features in planes other than those of the original CT slices themselves.

3.4.2 Filament Wound Bottle with Foam Core

Filament winding is another example of using fibers for performance gains over traditional structures. A composite bottle, 460 mm in diameter (18 inches), with a foam core, fabricated with a filament wound exterior wall and composite interior wall, is shown in Figure 3.4.2-1. The interior wall was made in two sections which were butted together and then bonded to a sleeve which overlapped the two butted wall sections.



Figure 3.4.2-1 Composite filament wound bottle with a foam core.

Several slices of the bottle were made to investigate potential disbonds and the condition of the foam core material. Figure 3.4.2-2 is a CT slice taken through the region of the bottle including the butt joint and sleeve. The foam core material is seen in this figure, along with an indicator marker just below "3 o'clock" in the figure. At about "5 o'clock" a gap in the wall material is indicated. This gap is too far away from the inner surface of the bottle to be the bond between the wall and the sleeve. It is a gap in the inner wall itself. Adjusting the window level to omit the lighter density materials, such as the core foam and the sleeve, permits further detail as to the condition of the inner wall itself. Figure 3.4.2-3 is the same slice with the window level increased to show only the denser materials in the figure. The wall gap, revealed in the previous figure, is seen to be more extensive, at "4 o'clock and 5 o'clock," with further indications at "10 o'clock" and just above "3 o'clock." No other NDE method is capable of giving this information on an enclosed structure such as this.

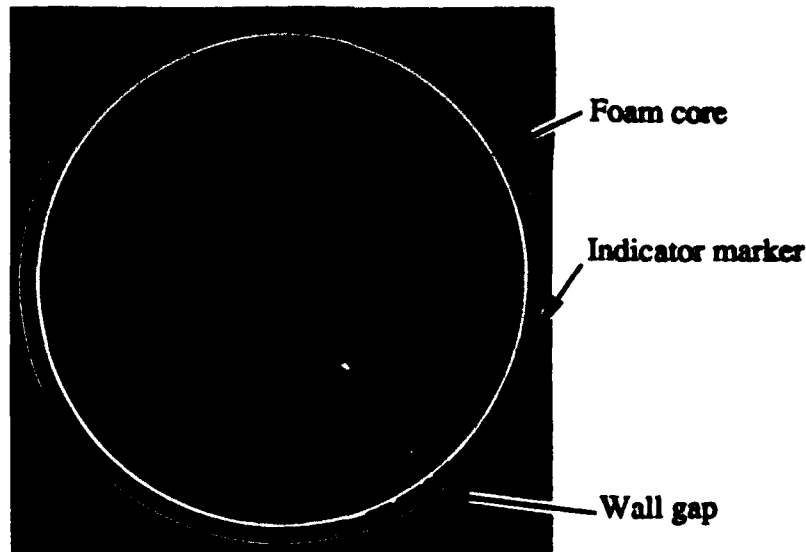


Figure 3.4.2-2 CT slice of the bottle.



Figure 3.4.2-3 CT slice of Figure 3.4.2-2 with contrast adjustment.

3.4.3 Wound Fiberglass Composite Ring

A second example of a wound component is a fiberglass composite ring, 156 mm (6 inches) in diameter and a 15-mm- (0.6-inch-) thick wall. The ring was examined for voids and general condition of the composite. A photograph of the ring is shown in Figure 3.4.3-1. Several CT slices of the ring were made. One is shown in Figure 3.4.3-2. This slice indicated voids between windings near the outer surface of the ring at about "6 o'clock" and "8 o'clock." The image also shows a number of low-density indications. In addition, the inner most portion of the ring is considerably less dense than the remainder of the ring. These features are quickly detected with CT, and give much more detail concerning the general condition of the ring and process effects than any other NDE method.



Figure 3.4.3-1 Photograph of fiberglass ring.

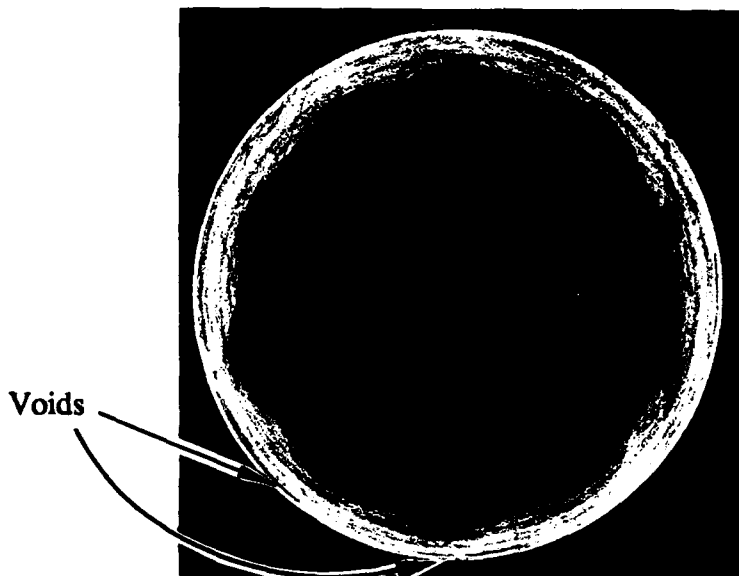


Figure 3.4.3-2 CT image of the ring showing voids in the windings.

3.5 Material Density/Consolidation

Material density and consolidation measurements are important in emerging material developments. In an earlier CTAD report, material consolidation was shown to correlate with shear strength in graphite epoxy [10], and in Section 3.3-1 consolidation was an important parameter in a graphite epoxy structure. This section discusses several other types of emerging materials and the usefulness of CT for their evaluation.

3.5.1 Structural Foam for Spar Manufacture

Structural foam is under consideration as a replacement for vacuum bag pressure systems in the manufacture of the interior of a composite helicopter blade spar. During the curing process of the laminate spar wall, the foam would supply the interior mechanical pressure to hold the dimensions of the composite spar wall. The foam is light weight and could remain in the blade, allowing the aircraft to simply "fly away" with the foam. Because it is intended for use in a flight structure, it is necessary to know the density variation, if any, prior to installing the foam in the spar wall.

Evaluation of test foam was performed on rectangular samples in two conditions: "green" and thermoformed. The thermoformed specimens are representative of those to be installed in the spar. Five green specimens, labelled B1 through B5, and six thermoformed specimens, labelled A1 through A6, were examined by CT. A photograph of the five green specimens mounted for CT scanning appears as Figure 3.5.1-1. As shown in the figure, all five of the green specimens were scanned simultaneously, as were the six thermoformed specimens.



Figure 3.5.1-1 Photograph of the five green specimens mounted for CT examination.

The green specimens were each 150 x 150 x 25 mm (6 x 6 x 1 inches), and the thermoformed specimens were 150 x 150 x 18 mm (6 x 6 x 0.7 inches). Each of the CT scans were taken through the center of the specimens directed through the short dimension (thickness). A CT

image of the green specimens is shown in Figure 3.5.1-2, revealing very little density variation. In this scan, the specimens are surrounded by a corrugated cardboard ring to reduce very soft X-rays from the beam and reduce image artifacts on the outside edges of the foam. The CT image of the thermoformed specimens is shown in Figure 3.5.1-3. There is considerable density variation through the thickness of these specimens, especially for samples 5 and 6, which are the two closest to the bottom of the figure. In both of the images, but more pronounced in Figure 3.5.1-3, the dotted inklines made by pen on the surface of the specimens to indicate the desired slice location are evident. They occur as small "blips" along the upper surfaces of specimens A1 through A6, and specimens B3 and B4. This gives an impressive indication of the sensitivity of the data to small density changes along a boundary.

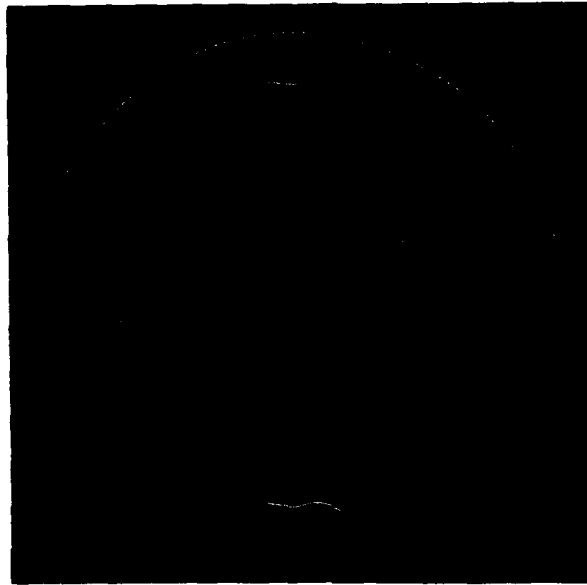


Figure 3.5.1-2 CT images of the "green" foam specimens.

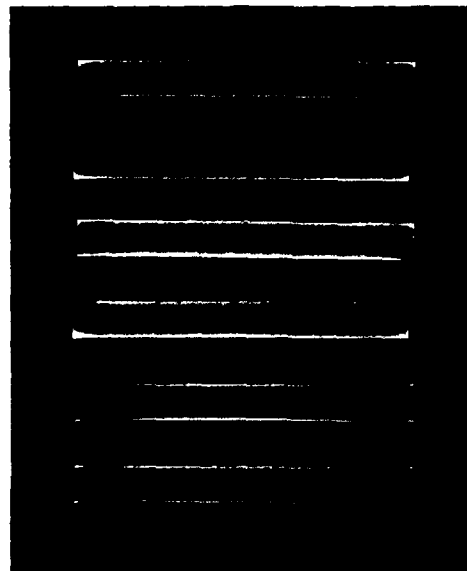


Figure 3.5.1-3 CT image of the thermoformed foam specimens.

The density data was plotted versus distance through the thickness of the two sets of specimens. These are shown as Figures 3.5.1-4 for the green specimens and 3.5.1-5 for the thermoformed specimens. The green specimens show density variations of 5-10 percent, and the thermoformed specimens variations of 15-25 percent. The calibration of the density was determined by including a carbon rod of 0.33 g/cm^3 in the slices.

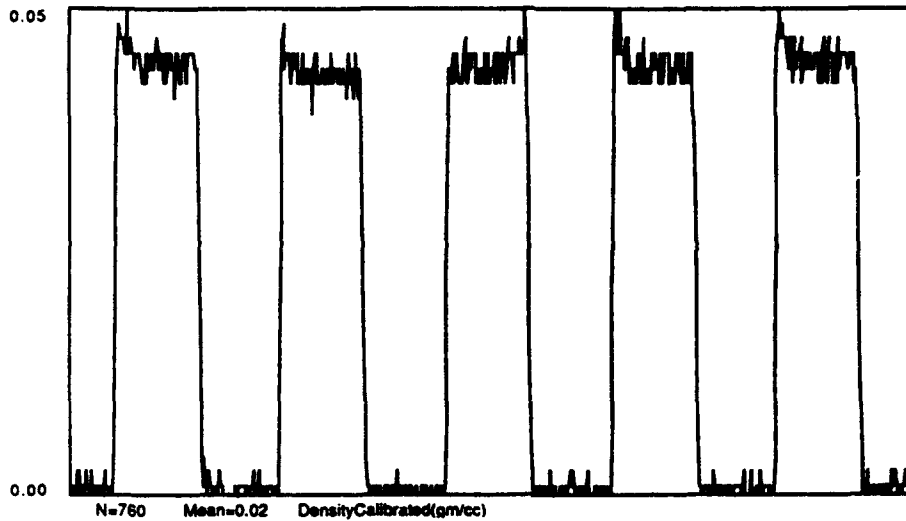


Figure 3.5.1-4 Density plots of "green" foam specimens.

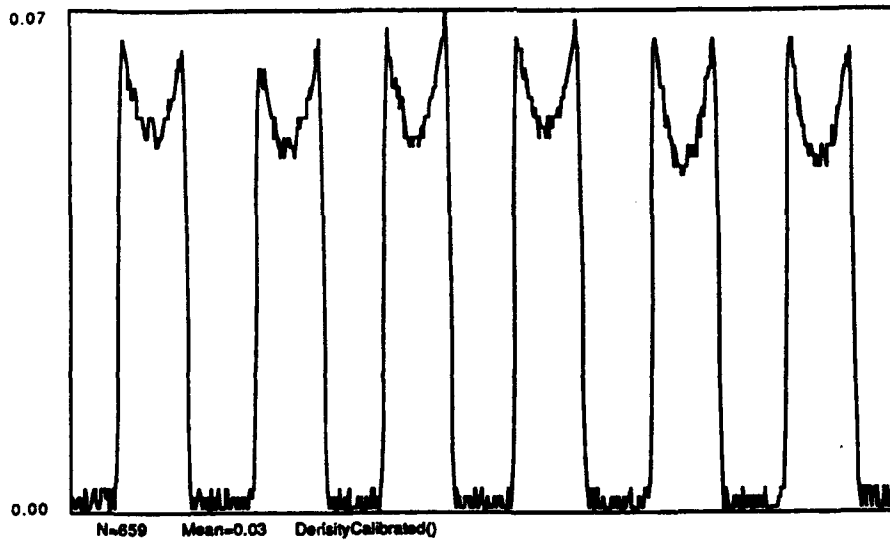


Figure 3.5.1-5 Density plots for thermoformed foam specimens

The CT data shows that the first curing process (thermoforming) clearly changed the density distribution of the material from being homogeneous to having a higher density at the edges.

This information was useful in determining the requirements for a viable foam, and in evaluating the potential of this particular foam to the proposed flight application. Future testing will consist of CT scanning of cured thermoformed foam in a test enclosure simulating a spar interior.

3.5.2 Fibrous Ceramic Tile

Fibrous ceramics are being developed for high-temperature insulation in aerospace applications. An example is a low-density chopped fiber ceramic tile specimen embedded into a titanium (Ti) alloy honeycomb. A photograph of a small specimen is shown in Figure 3.5.2-1. The honeycomb provides strength for the tile, and contains holes through which the ceramic should connect when it is "poured." The Ti honeycomb does not quite extend all the way through the thickness of the specimen, so it is not visible from one side.

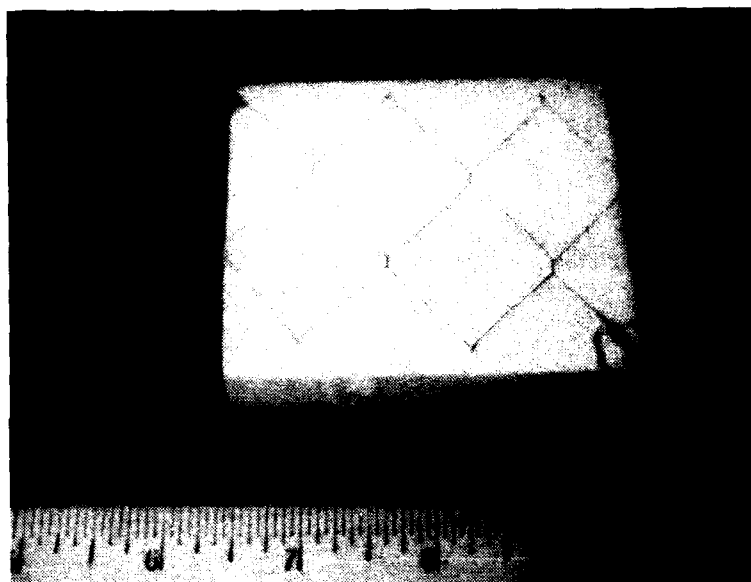


Figure 3.5.2-1 Photograph of fibrous ceramic tile.

CT was used to determine if the ceramic had completely flowed into the holes contained in the Ti honeycomb. When the part was scanned with the CT slice parallel to the surface shown in Figure 3.5.2-1, the crisscross pattern of the titanium could be seen within the ceramic interior. Figure 3.5.2-2 is an example of one of these images. Voids as well as the density distribution of the ceramic were easily imaged. However, the streak artifacts caused by the titanium eliminated the possibility of measuring the density in the holes. A series of slices were taken (five slices, 4 mm (0.16 inches) apart), the last of which just missed the titanium, going just below it, as shown in Figure 3.5.2-3. This slice indicates the density variation of the fibrous ceramic near the titanium. Apparently, the flow characteristics close to the titanium reduces the fiber concentration just below the grid.



Figure 3.5.2-2 CT image in fibrous ceramic tile.

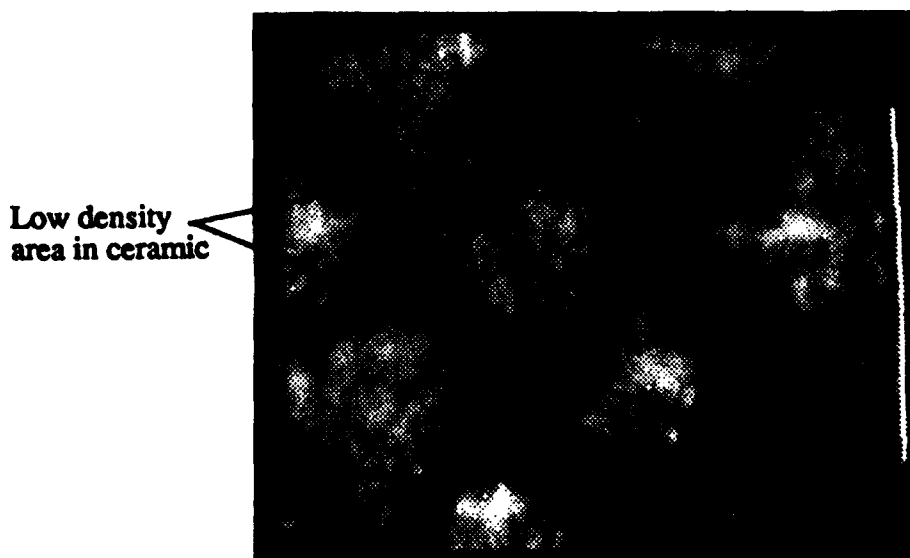


Figure 3.5.2-3 CT image in fibrous ceramic tile.

The first scans taken through the smallest dimension of the specimen were disappointing, because the artifacts from the Ti masked the information in the holes. Aluminum blocks, 25 mm (1 inch) thick, were placed on both sides of the panel to equalize the X-ray paths and reduce the artifacts along the Ti. This "trick" worked, as the region inside the holes could now be imaged. Figure 3.5.2-4 is an example of one of the slices. The image shows that the ceramic flowed into the holes because there is no reduction in measured CT density. In this figure, the holes in the titanium appear as "c" and "o" shapes. Within these holes, the material has the same apparent density as the ceramic in other regions of the specimen. These CT scans provided a materials group with the information needed to determine that this process allowed connecting of the ceramic through the holes in the honeycomb. No other nondestructive inspection method was able to satisfactorily provide this information.

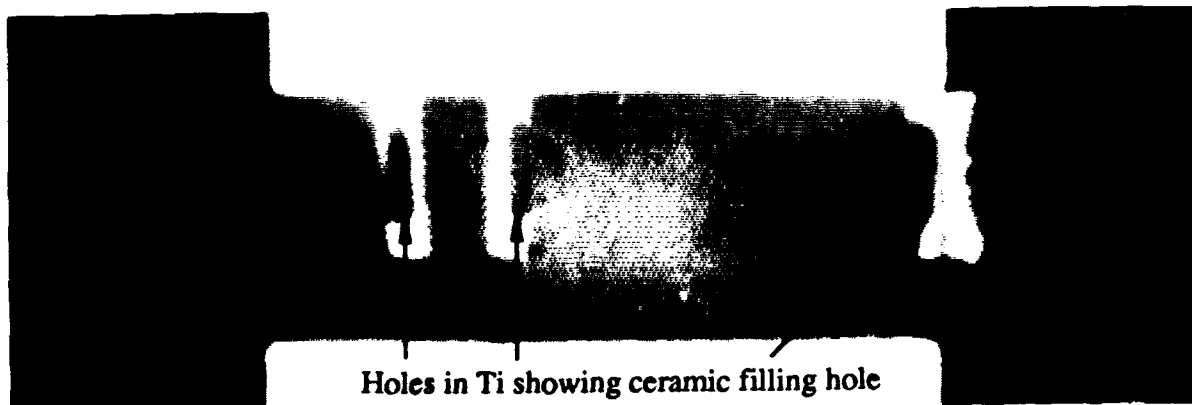


Figure 3.5.2-4 CT image in fibrous ceramic tile.

3.5.3 High Temperature Coated Specimens

Coatings are critical for high-temperature applications. The coatings and processes surrounding their use can benefit from CT evaluation. For example, small SiC coated carbon-carbon samples were fabricated with different candidate thermocouple to composite substrate attachment schemes to determine the best type of thermocouple connection for high-temperature instrumentation of a full scale test component. Figure 3.5.3-1 is a photograph of two of the specimens. The larger specimen (specimen A) contains thermocouple attachment points made by inserting iridium wires in 1.25-mm-diameter holes with an alumina based cement. Specimen B contains a silicon nitride insert cemented to the top of the coating. These specimens, along with several others, were subjected to a series of high-temperature test cycles similar to the one expected for the full-scale test. Although the samples were examined with CT only after high-temperature cycling, it would have been preferable to CT scan both before and after testing to better quantify the effects of the thermal cycling. The purpose of the CT effort was to obtain an accurate picture of the material loss due to oxidation of the composites. This oxidation would be attributable to leakage in the coating, arising from the attachment process of the thermocouples. The samples were all weighed before and after testing, so the samples which lost mass were already known. What was not known was the actual leakage points or spatial extent of the loss. CT data provided this information, as shown in Figures 3.5.3-2 and 3.5.3-3.

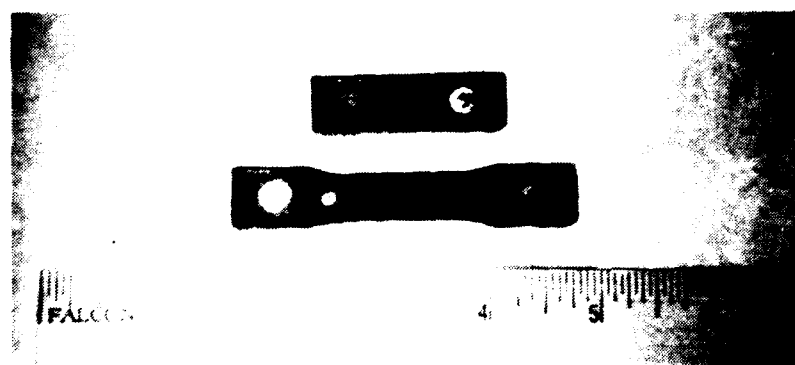


Figure 3.5.3-1 Photograph of two of the coated specimens.

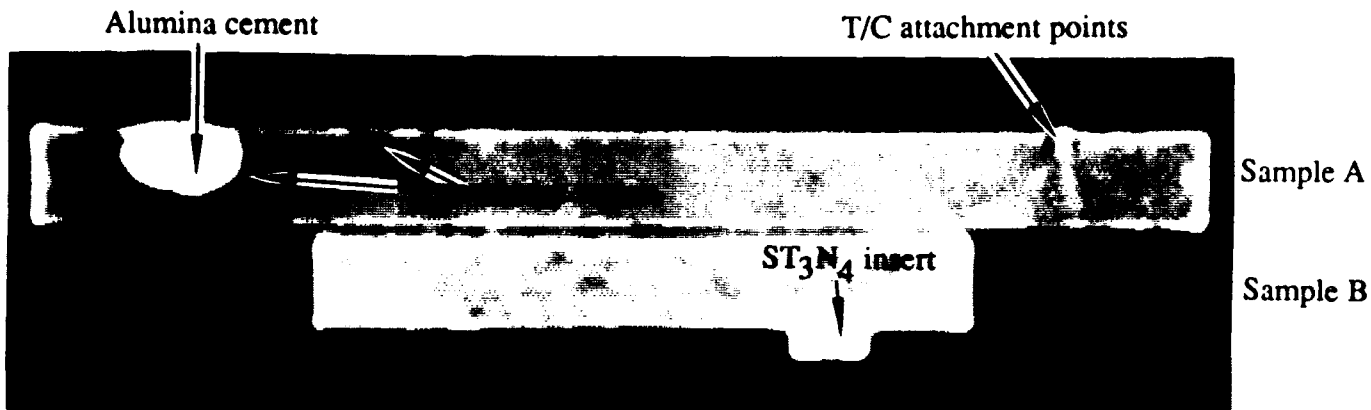


Figure 3.5.3-2 CT image of specimens shown in Figure 3.5.3-1.

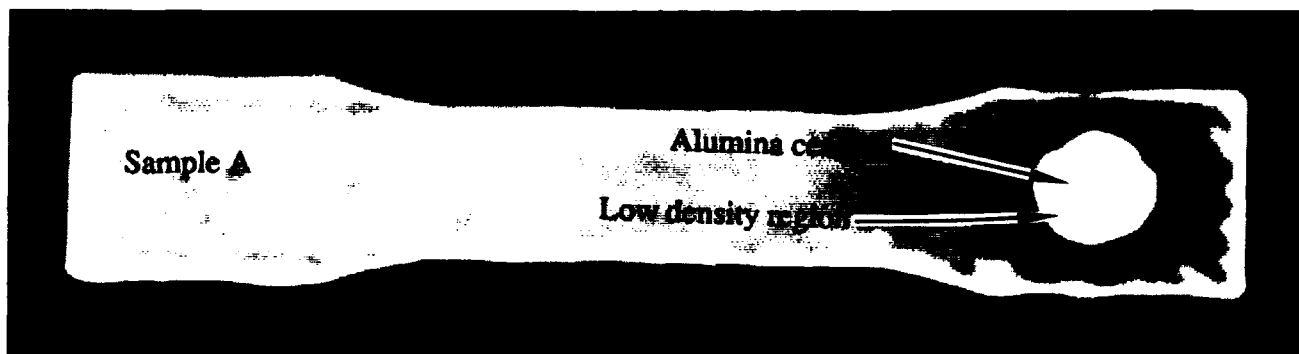


Figure 3.5.3-3 CT image taken perpendicular to Figure 3.5.3-2.

Figure 3.5.3-2 is a CT slice taken through the two specimens shown in Figure 3.5.3-1. The larger specimen (specimen A) contains two thermocouple attachment points. Oxidation damage can be seen clearly around the left point (which had been subjected to 25 cycles), and is barely visible near the right attachment point (which had been subjected to 45 cycles). Figure 3.5.3-3 is a CT slice taken perpendicular to Figure 3.5.3-2 just below the coating of specimen A. This slice reveals the amount of oxidation around the thermocouple attachment points. The left end of sample A contains a previous attachment point that failed under initial thermal cycling, but was "repaired" by removing and filling the oxidized area with an alumina paste. The repair was not successful, as leakage paths around the paste allowed further oxidation upon subsequent thermal cycling.

It turned out that once the coatings were penetrated, unrecoverable damage in the form of oxidation to the specimen always resulted. Thus, whether the thermocouple was installed in the sample by drilling a hole through the coating, or in an insert which was installed in the sample

and subsequently overcoated, damage to the interior of the specimen always occurred. CT effectively became a means of accurately defining how the damage occurs, as well as positively disqualifying several approaches for thermocouple attachment. The information provided by the CT scans reduced the cycle time for the process of arriving at the selected method by allowing fewer specimens to be made, and requiring less time for both people and equipment. The method finally chosen was to cement the thermocouple to a coated specimen.

3.5.4 Aluminum MMC Rods

Metal matrix composite (MMC) development can benefit from CT evaluation of material consolidation. An example is aluminum metal matrix composite rods provided by the Solidification Laboratory of the University of Alabama. The objective of the project is to understand particle behavior at the solidifying interface of the matrix. Ground experiments are not capable of distinguishing between several kinds of forces due to the presence of too strong a gravity influence. Microgravity experiments in space will clear up this ambiguity, and hopefully confirm a kinetic model. The project needed a method of determining the condition of candidate flight specimens, as to the homogeneity of their interior.

The rods are essentially aluminum alloy (1 percent by weight magnesium) matrix containing 2 percent silicon carbide particles. The sizes of the particles are approximately 0.060 mm (0.002 inch) in diameter. A photograph of the two rods scanned is shown in Figure 3.5.4-1. The thicker rod is about 8 mm (0.3 inch) in diameter, and the thinner one is about 4 mm (0.16 inch) in diameter. Before flight, it was of interest to confirm that the samples were of acceptable homogeneity on an appropriate scale.

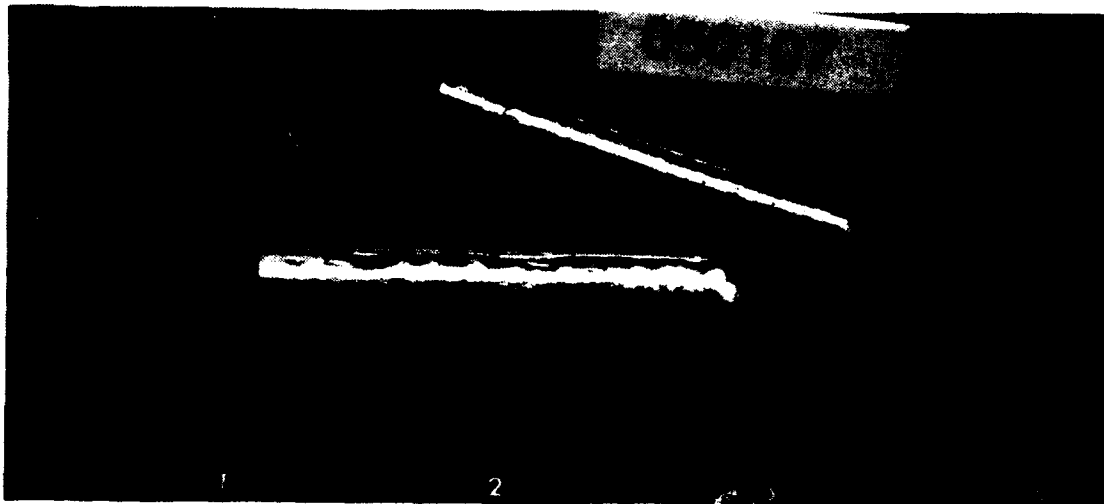


Figure 3.5.4-1 Photograph of Al MMC rods.

The rods were scanned on a high-resolution (> 4 lp/mm) CT system. Multiple CT slices, with slice thickness of 0.25 mm (0.01 inch), were taken through the circular cross section for the small and large rods. Figure 3.5.4-2 is a CT image of the small rod and Figure 3.5.4-3 is a CT image of the large rod. There are obvious voids in both of the specimens. The SiC particles are detected as light dots in the image. The granularity associated with each of the slices is the approximate size of the particles. The amount of voiding was consistent along the rods over the

CT slice series. The mean and standard deviation of the rod material showed no significant variation along the rods.

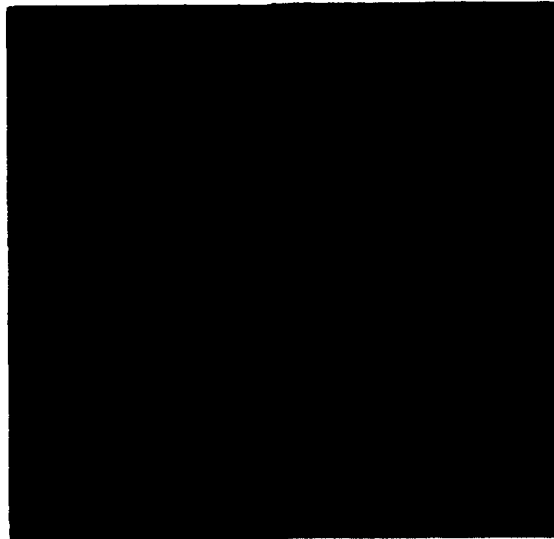


Figure 3.5.4-2 CT image of small aluminum MMC rod.



Figure 3.5.4-3 CT image of large aluminum MMC rod.

The results of these tests indicate that CT is an excellent technique for evaluating material consolidation and uniformity in the rods to be subsequently found on the flight experiments. In this case, CT proved to be the only way in which the MMC specimens could be quantitatively assessed nondestructively.

4.0 CONCLUSIONS

The evaluation of the applicability of CT to emerging materials and processes development indicates that CT is useful, but the cost benefits are realized in terms which are difficult to quantify: reduced risk, reduced cycle time for development, and increased design options. Figure 4.1-1 summarizes the conclusions.

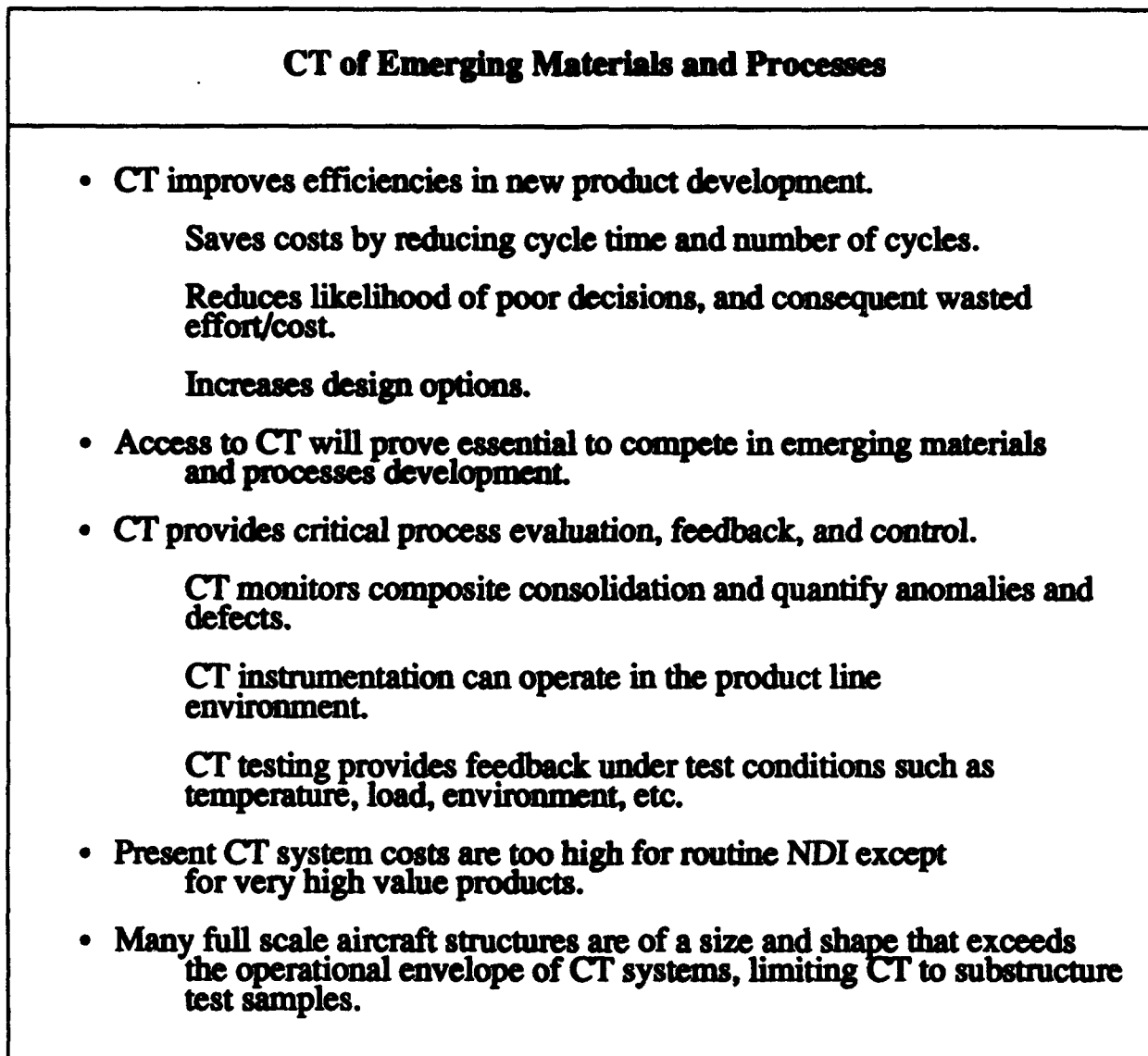


Figure 4.1-1 Emerging materials and processes conclusions.

New materials or products usually involve an iterative cycle of manufacture and testing to bring the process under control. CT provides important information about the product to the manufacturing engineer which can accelerate this process. CT can be considered as an enabling technology for the development of new materials, products, or manufacturing processes. Accelerated development often results in significant initial cost savings and reduced risk of poor

designs being manufactured. It can result in enormous savings over the lifetime of a program. CT is a tool to be used in the "Concurrent Engineering" process. Because of this, access to CT will be essential to companies involved in emerging materials processing development activities.

CT can be used for process evaluation feedback and control of a manufacturing process as part of a "Total Quality Management" program. The CT measurements of X-ray linear attenuation coefficient (directly related to density and a function of atomic number) and the accurate dimensional information provided are ideal for making important statistical measurements as well as for defect characterization in many emerging materials and process developments. Developers of advanced materials should plan for CT availability when costing the development of new materials or products. The ultimate goal of using CT for process evaluation, feedback and control will be to include CT in the product line. For example, on-line CT was considered a part of an earlier CTAD report for use on pultrusion manufactured products [4]. In-line CT will require developments in lower cost CT equipment. High-throughput medical CT technology holds promise for applications on in-line operations, where the object is of a size that can fit within the scanner operating diameter.

CT measurements are very useful as part of an environmental test program. CT has been used successfully in the example stories of this report between stages of environmental tests. CT can be performed during environmental or load testing with proper equipment. Such measurements can be particularly useful for material testing when the environment extremes exceed the capabilities of conventional test instruments such as strain gauges and/or vision systems.

CT system and operation costs are presently too high for routine examination except for the most costly products. Rather, CT is an enabling technology for product development. CT system costs will need to be reduced to the throughput costs of traditional NDI for CT to be implemented as an NDI tool. There are opportunities for this possibility in the future with high throughput, low-cost CT technology currently being developed. Volumetric CT imaging will offer some advantages. For small (< 50 mm (2 inches)) test samples, some high-resolution CT systems have capital and operating costs that are low enough to be used for routine examination.

The geometry of many full scale aircraft composite and advanced material structures tend to exceed the operational regimes of conventional (360°) access CT techniques because of the overall assembly size and aspect ratio. Because of this, CT will apply to substructure, subsection testing or small material components.

5.0 REFERENCES

1. R. H. Bossi, R. J. Kruse, and B. W. Knutson, "Computed Tomography of Electronics," WRDC-TR-89-4112, December 1989.
2. R. H. Bossi, J. L. Cline, and B. W. Knutson, "Computed Tomography of Thermal Batteries and Other Closed Systems," WRDC-TR-89-4113, December 1989.
3. R. H. Bossi, J. L. Cline, E. G. Costello, and B. W. Knutson, "X-Ray Computed Tomography of Castings," WRDC-TR-89-4138, March 1990.
4. R. H. Bossi, K. K. Coopriider, and G. E. Georgeson, "X-Ray Computed Tomography of Composites," WRDC-TR-90-4014, July 1990.
5. P. Burstein and R. H. Bossi, "A Guide to Computed Tomography System Specifications," WRDC-TR-90-4026, August 1990.
6. R. H. Bossi and R. J. Kruse, "X-Ray Tomographic Inspection of Printed Wiring Assemblies and Electrical Components," WRDC-TR-90-4091, October 1990.
7. G. E. Georgeson and R. H. Bossi, "X-Ray Computed Tomography of Full-Scale Castings," WL-TR-91-4049, October, 1991.
8. Richard H. Bossi and Gary E. Georgeson, "Computed Tomography Analysis of Castings," WL-TR-91-4121, January, 1992.
9. Alan R. Crews and Richard H. Bossi, "Computed Tomography for Whole System Inspection," WL-TR-91-4109, May, 1992.
10. Gary E. Georgeson and Richard H. Bossi, "Computed Tomography for Advanced Materials and Processes," WL-TR-91-4101, June, 1992.
11. Richard H. Bossi, John L. Cline and Gary E. Georgeson, "High Resolution X-Ray Computed Tomography," WL-TR-91-4102, July, 1992.
12. Richard H. Bossi, Alan R. Crews and Gary E. Georgeson, "X-Ray Computed Tomography for Failure Analysis," WL-TR-92-4017, August 1992.
13. Gary E. Georgeson, Alan R. Crews and Richard H. Bossi, "X-Ray Computed Tomography for Casting Development," WL-TR-92-4032, September 1992.
14. Alan R. Crews, Richard H. Bossi, and Gary E. Georgeson, "X-Ray Computed Tomography for Geometry Acquisition," WL-TR-93-4036, March 1993.
15. Richard H. Bossi and William Shepherd, "X-Ray Computed Tomography for Failure Analysis Investigations," WL-TR-93-4047, May 1993.
16. Gary E. Georgeson, Raymond D. Rempt, and Richard H. Bossi, "X-Ray Computed Tomography Demonstrations for Castings," WL-TR-93-4048, May 1993.